Monthly Notices
of the
ROYAL ASTRONOMICAL SOCIETY

MNRAS **437,** 1241–1258 (2014)
Advance Access publication 2013 November 20

doi:10.1093/mnras/stt1944

NGC 1817, NGC 2141 and Berkeley 81: three BOCCE clusters of intermediate age⋆

P. Donati,[1,2]† G. Beccari,[3] A. Bragaglia,[2] M. Cignoni[1,2,4] and M. Tosi[2]

[1]*Dipartimento di Fisica e Astronomia, via Ranzani 1, I-40127 Bologna, Italy*
[2]*INAF – Osservatorio Astronomico di Bologna, via Ranzani 1, I-40127 Bologna, Italy*
[3]*European Southern Observatory, Alonso de Cordova 3107, 19001 Santiago de Chile, Chile*
[4]*Space Telescope Science Institute, Baltimore, MD 21218, USA*

Accepted 2013 October 8. Received 2013 October 7; in original form 2013 September 4

ABSTRACT

In this paper we analyse the evolutionary status of three open clusters: NGC 1817, NGC 2141 and Berkeley 81. They are all of intermediate age, two are located in the Galactic anticentre direction while the third one is located in the Galactic Centre direction. All of them were observed with Large Binocular Camera at Large Binocular Telescope using the Bessel *B*, *V* and *I* filters. The cluster parameters have been obtained using the synthetic colour–magnitude diagram (CMD) method, i.e. the direct comparison of the observational CMDs with a library of synthetic CMDs generated with different evolutionary sets (Padova, FRANEC and FST). This analysis shows that NGC 1817 has subsolar metallicity, age between 0.8 and 1.2 Gyr, reddening $E(B-V)$ in the range 0.21 and 0.34 and distance modulus $(m-M)_0$ of about 10.9; NGC 2141 is older, with age in the range 1.25 and 1.9 Gyr, $E(B-V)$ between 0.36 and 0.45, $(m-M)_0$ between 11.95 and 12.21 and subsolar metallicity; Berkeley 81 has metallicity about solar, with age between 0.75 and 1.0 Gyr, has reddening $E(B-V) \sim 0.90$ and distance modulus $(m-M)_0 \sim 12.4$. Exploiting the large field of view of the instrument we derive the structure parameters for NGC 2141 and Berkeley 81 by fitting a King profile to the estimated density profile. Combining this information with the synthetic CMD technique we estimate a lower limit for the cluster total mass for these two systems.

Key words: Hertzsprung–Russell and colour–magnitude diagrams – Galaxy: disc – open clusters and associations: general – open clusters and associations: individual: Berkeley 81 – open clusters and associations: individual: NGC 1817 – open clusters and associations: individual: NGC 2141.

1 INTRODUCTION

This paper is part of the long-term Bologna Open Clusters Chemical Evolution (BOCCE) project, aimed at precisely and homogeneously derive the fundamental properties of a large sample of open clusters (OCs), and described in detail by Bragaglia & Tosi (2006). The ultimate goal of the BOCCE project is to get insight on the formation and evolution of the Galactic disc, and OCs are among the best tracers of the disc properties (e.g. Friel 1995). We have already analysed photometric data for 31 OCs (see Bragaglia & Tosi 2006; Cignoni et al. 2011; Donati et al. 2012; Ahumada et al. 2013, and references therein), and derived their age, distance and reddening from the comparison of their colour–magnitude diagrams (CMDs) with synthetic ones based on three sets of stellar evolution models (see Bragaglia & Tosi 2006).

In this paper we discuss NGC 1817 (Galactic coordinates $l = 207.^\circ8, b = 2.^\circ6$), NGC 2141 ($l = 214.^\circ2, b = 1.^\circ9$) and Berkeley 81 (Be 81; $l = 227.^\circ5, b = -0.^\circ6$). These clusters have been selected because they could be targets of the *Gaia*–ESO Survey (GES; see Gilmore et al. 2012 for a description). The GES is an on-going public spectroscopic survey with Fibre Large Array Multi Element Spectrograph (FLAMES) at Very Large Telescope (VLT), that will obtain high-resolution GIRAFFE and UVES spectra of about 10^5 stars of all Milky Way components, including stars in about 100 OCs and associations. For all the GES cluster targets we need photometry and precise astrometry covering all the FLAMES field of view (FoV; diameter of 25 arcmin) to properly point the fibres.

⋆ Based on observations collected at the Large Binocular Telescope (LBT). The LBT is an international collaboration among institutions in the United States, Italy and Germany. LBT Corporation partners are: The University of Arizona on behalf of the Arizona University system; Istituto Nazionale di Astrofisica, Italy; LBT Beteiligungsgesellschaft, Germany, representing the Max-Planck Society, the Astrophysical Institute Potsdam and Heidelberg University; The Ohio State University and The Research Corporation, on behalf of The University of Notre Dame, University of Minnesota and University of Virginia.

† E-mail: paolo.donati4@unibo.it

Table 1. List of the main properties of the three clusters found in literature. The true distance modulus $(m - M)_0$ is evaluated from literature values after applying the same extinction law adopted in this paper ($R_V = 3.1$).

Cluster	$E(B-V)$	$(m-M)_0$	Age	Metallicity	Reference
NGC 1817	0.28	11.3 ± 0.4	∼Hyades	Less than Hyades	Harris & Harris (1977)
	0.27	10.9 ± 0.6	1.1 Gyr	[Fe/H] $= -0.34 \pm 0.26$	Balaguer-Núñez et al. (2004)
				[Fe/H] $= -0.33 \pm 0.09$	Parisi et al. (2005)
				[Fe/H] $= -0.38 \pm 0.04$	Friel & Janes (1993)
				[Fe/H] $= -0.07 \pm 0.04$	Jacobson et al. (2009)
				[Fe/H] $= -0.16 \pm 0.03$	Jacobson et al. (2011)
				[Fe/H] $= -0.11 \pm 0.05$	Reddy, Giridhar & Lambert (2012)
NGC 2141	0.3	13.17	NGC 2477 < age < M67		Burkhead et al. (1972)
	0.35 ± 0.07	13.08 ± 0.16	2.5 Gyr	$Z = 0.004$–0.008	Rosvick (1995)
	0.40	12.90 ± 0.15	2.5 Gyr	[Fe/H] $= -0.43 \pm 0.07$	Carraro et al. (2001)
				[Fe/H] $= -0.39 \pm 0.11$	Friel & Janes (1993)
				[Fe/H] $= -0.18 \pm 0.15$	Yong et al. (2005)
				[Fe/H]$= +0.00 \pm 0.16$	Jacobson et al. (2009)
Be 81	1.0	12.5	1 Gyr	Solar	Sagar & Griffiths (1998)
				[Fe/H] $= -0.15 \pm 0.11$:	Warren & Cole (2009)

Such adequate photometry was not yet available for NGC 2141, Be 81 and NGC 1817, and we acquired it on purpose with Large Binocular Telescope (LBT).

NGC 2141 and NGC 1817 are anticentre clusters, whilst Be 81 lies towards the Galactic Centre,[1] so they are particularly interesting to study the radial distribution of the disc properties. In Table 1 we report a consistent summary of all the parameters available in the literature for the three clusters. It is apparent that they do not agree with each other, and a more precise analysis is called for.

NGC 1817. Its richness, distance from the Galactic plane (−400 pc) and metallicity make this cluster particularly interesting. In fact, NGC 1817 has been the target of many photometric studies, starting from Arp & Cuffey (1962) and Purgathofer (1961), who obtained shallow photographic CMDs, including only stars at the main-sequence turn-off (MSTO) and some giants. Harris & Harris (1977) acquired photographic *UBV* data, providing a well defined MS and red clump (RC), and derived distance, reddening (see Table 1), age similar to the Hyades and a low metallicity. Balaguer-Núñez et al. (2004b) performed deep, wide field photometry in the Strömgren system ($uvby - \mathrm{H}\beta$), covering an area of 65×40 arcmin^2 and building on the proper motion and membership analysis by Balaguer-Núñez, Tian & Zhao (1998). For the cluster members they derived the parameters listed in Table 1. A subsolar metallicity was derived by Parisi et al. (2005) on the basis of Washington photometry.

Spectroscopic analyses were made using low-resolution spectra by Friel & Janes (1993) and high-resolution ones by Jacobson, Friel & Pilachowski (2009), Jacobson, Pilachowski & Friel (2011) and Reddy et al. (2012) for different cluster stars. Despite showing different results all these studies point to a slightly subsolar metallicity (see Table 1). Crucial information on radial velocities (RVs), membership and binary stars were given by Mermilliod et al. (2003, 2007), and Mermilliod, Mayor & Udry (2008).

NGC 2141. It is a rich cluster, subject of several studies in the past. Burkhead, Burgess & Haisch (1972) obtained photoelectric and photographic *UBV* data, barely reaching below the MSTO; they determined the distance modulus and reddening listed in Table 1, and an age intermediate between those of M67 and NGC 2477. Rosvick (1995) observed an area of 173 arcmin^2 with *VI* filters and a smaller area with *JHK*. Her CMD reached about 4 mag below the MSTO, and showed a large scatter, interpreted in terms of both field star contamination and differential reddening (DR). Rosvick (1995) determined the reddening, distance modulus, metallicity and age listed in Table 1 from a fit with the Bertelli et al. (1994) isochrones. The latest photometric data for this cluster have been presented by Carraro et al. (2001), who acquired *BV* and *JK* data. Their optical CMD extends to $V \sim 21.5$, while the IR CMD reaches about 2 mag below the MSTO. They estimated the metallicity from the IR photometry, deriving best-fitting age and distance, based on the Girardi et al. (2000) isochrones (see Table 1).

Spectroscopic analyses of cluster stars were made by different authors: Friel & Janes (1993) and Minniti (1995) used low-resolution spectra, while Yong, Carney & Teixera de Almeida (2005) and Jacobson et al. (2009) used high-resolution ones. They found different values for the cluster metallicity from solar to subsolar (see Table 1). Jacobson et al. (2009) discussed the possible sources for the discrepancy and thoroughly analysed the literature findings. In summary, this cluster has a metallicity near solar or slightly lower, and this information will be used here to constrain the choice of the cluster's parameter.

Be 81. BVI photometry of part of Be 81 has been presented by Sagar & Griffiths (1998). They argued for the absence of significant DR from the CMDs of different regions, and attributed the width of the MS to the presence of field stars, binaries and variables. They derived a cluster radius of 2.7 ± 0.2 arcmin, and the reddening, distance modulus and age listed in Table 1, using the Bertelli et al. (1994) isochrones with solar metallicity.

The metallicity of Be 81 was determined from calcium triplet (CaT) spectroscopy by Warren & Cole (2009). Their subsolar value is however quite uncertain, since they were unable to convincingly define the cluster mean RV, due to the huge contamination by field stars. The GES spectra will thus be crucial to infer its actual metallicity.

This paper is organized as follows. Observations and the resulting CMDs are presented in Section 2; the estimation of the clusters centre in Section 3; DR is discussed in Section 4; the derivation of their age, distance, reddening and metallicity using comparison to synthetic CMDs in Section 5. Discussion and summary can be found in Section 6.

[1] On the basis of the moduli derived in the following sections their distances from the Galactic Centre are $R_{GC} \simeq 9.5$ kpc for NGC 1817, $R_{GC} \simeq 12$ kpc for NGC 2141 and $R_{GC} \simeq 5.7$ kpc for Be 81.

Table 2. Logbook of the observations. The listed coordinates refer to the telescope pointings.

Cluster name	RA ($^{h\,m\,s}$) (J2000)	Dec. ($^\circ\ '\ ''$) (J2000)	Date	*B* Exp. time (s)	*V* Exp. time (s)	*I* Exp. time (s)	Seeing (arcsec)
NGC 1817	05 12 41	16 44 30	2011 October 24	1, 3 × 5, 3 × 90	1, 3 × 5, 3 × 60	1, 3 × 5, 3 × 60	1
NGC 2141	06 02 57	10 27 27	2011 October 21	1, 3 × 5, 3 × 90	1, 3 × 5, 3 × 60	1, 3 × 5, 3 × 60	1
Be 81	19 01 41	−00 27 40	2011 October 20	1, 3 × 5, 3 × 90	1, 3 × 5, 3 × 60	1, 3 × 5, 3 × 60	1

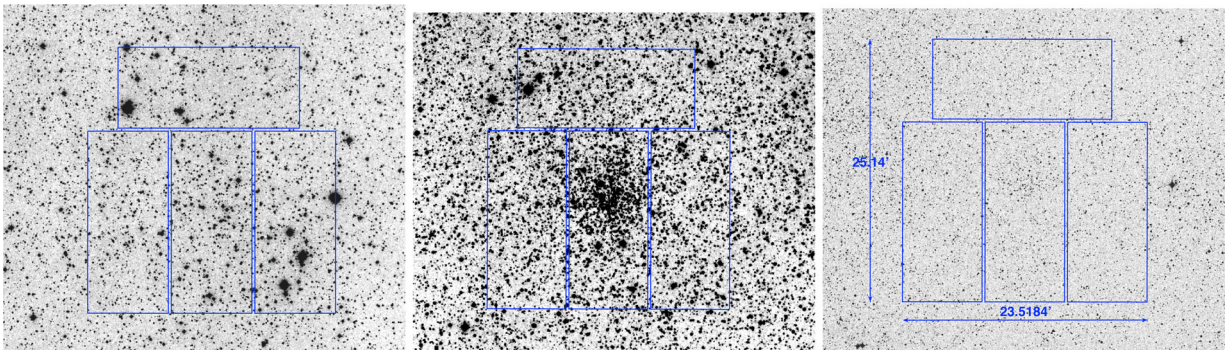

Figure 1. The FoVs of the three clusters, NGC 1817, NGC 2141 and Be 81, from left to right. In the last map on the right we highlight the dimension of the FoV in arcminutes. All these images were downloaded from the DSS SAO catalogue in the GSSS bandpass 6 (V495). North is up and east is left.

2 THE DATA

The three clusters were observed in service mode at the LBT on Mt. Graham (Arizona) with the Large Binocular Camera (LBC) in 2011 (see Table 2 for details). There are two LBCs, one optimized for the UV-blue filters and one for the red-IR ones, mounted at each prime focus of the LBT. Each LBC uses four EEV chips (2048 × 4608 pixels) placed three in a row, and the fourth above them and rotated by 90°(see Fig. 1). The FoV of LBC is equivalent to 22 × 25 arcmin^2, with a pixel sampling of 0.23 arcsec. The clusters were positioned in the central chip (#2) of the LBCs CCD mosaic (see Fig. 1). We observed in the *B* filter with the LBC-Blue camera and in *V* and *I* with the LBC-Red one. No dithering pattern was adopted. Table 2 gives the log of the observations. The seeing was good (about 1 arcsec), and the airmass of the exposures was in the range 1.0–1.3. Landolt fields were observed to perform our own calibration to the Johnson–Cousins system.

2.1 Data reduction

The raw LBC images were corrected for bias and flat-field, and the overscan region was trimmed using a pipeline specifically developed for LBC image pre-reduction by the Large Survey Center (LSC) team at the Rome Astronomical Observatory.[2] The source detection and relative photometry was performed independently on each *B*, *V* and *I* image, using the point spread function (PSF)-fitting code DAOPHOTII/ALLSTAR (Stetson 1987, 1994). We sampled the PSF using the highest degree of spatial variability allowed by the programme because the images are affected by severe spatial distortion. This procedure is adopted in other papers of this series and is proven to be effective to well sample the PSF on the whole frame. Giallongo et al. (2008) showed that the geometric distortion, of pin-cushion type, is always below 1.75 per cent even at the edge of the field. At any rate, for our purposes we mostly use the inner area of the FoV where a distortion up to only 1 per cent is expected. Moreover, the energy concentration of the instrumental PSF is very good: 80 per cent of the energy is enclosed in a single CCD pixel in the *B* band and in 2 × 2 pixels in the *V*, *I* bands.

The brightest stars, saturated in the deepest images, where efficiently recovered from the short exposure images. The weighted average of the independent measures obtained from the different images was adopted as the final values of the instrumental magnitude (basing the weight on the error). More than 200 stars from the Two Micron All Sky Survey (2MASS) catalogue (Skrutskie et al. 2006) where used as astrometric standards to find an accurate astrometric solution and transform the instrumental positions, in pixels, into J2000 celestial coordinates for each chip. To this aim we adopted the code CATAXCORR, developed by Paolo Montegriffo at the INAF – Osservatorio Astronomico di Bologna. The rms scatter of the solution was about 0.1 arcsec in both RA and Dec.

We derived the completeness level of the photometry by means of extensive artificial stars experiments following the recipe described in Bellazzini et al. (2002) and adopted in other papers of this series. About 10^5 artificial stars were used to derive photometric errors and completeness in *B*, *V* and *I* exposures for the central chip. The results are shown in Table 3.

2.2 Calibration and comparison with previous data

The calibration to the Johnson–Cousins photometric system was obtained using standard stars (Landolt 1992) obtained in the same observing nights. Landolt fields SA 98, SA 101, SA 113L1 and L92 were observed at different airmasses: in the range 1.2–1.9 during the nights of 2011 October 20 and 21, and in the range 1.2–1.5 during the third night. It was not possible to derive a calibration equation for each chip. So, we used the same one for all the four CCDs. The adopted calibration equation is the following:

$$(M - m_{\rm i}) = {\rm zp} + k\,C{\rm i},$$

where *M* is the magnitude in the standard photometric system, $m_{\rm i}$ the instrumental magnitude, zp the zero-point and *k* describes the linear dependence from the instrumental colour $C_{\rm i}$. We adopted the

[2] LSC website: http://lsc.oa-roma.inaf.it/

Table 3. Completeness level for calibrated *B*, *V* and *I* magnitudes.

	NGC 1817 ($d < 5$ arcmin)			NGC 2141 ($d < 4$ arcmin)			Be 81 ($d < 2$ arcmin)		
Bin	*B*	*V*	*I*	*B*	*V*	*I*	*B*	*V*	*I*
16.5	–	100.0 ± 1.0	–	–	100.0 ± 1.3	100.0 ± –	–	–	100.0 ± 3.0
17.0	100.0 ± 1.7	100.0 ± 1.8	100.0 ± 1.2	–	97.1 ± 1.4	100.0 ± 1.2	–	100.0 ± 6.0	84.9 ± 2.9
17.5	100.0 ± 1.4	100.0 ± 1.5	95.3 ± 1.1	100.0 ± 1.2	97.1 ± 1.4	95.7 ± 1.1	–	97.7 ± 5.5	77.6 ± 2.2
18.0	100.0 ± 1.9	96.1 ± 1.4	94.4 ± 1.0	97.4 ± 1.4	97.4 ± 1.2	94.7 ± 1.0	100.0 ± 8.2	94.2 ± 3.9	78.1 ± 1.9
18.5	100.0 ± 1.6	95.4 ± 1.4	92.5 ± 1.0	97.1 ± 1.4	96.7 ± 1.2	93.7 ± 0.9	98.5 ± 7.5	93.4 ± 3.6	69.6 ± 1.4
19.0	96.0 ± 1.6	95.9 ± 1.3	87.5 ± 0.9	96.8 ± 1.2	95.9 ± 1.2	90.8 ± 0.9	95.2 ± 4.5	92.2 ± 2.9	64.9 ± 1.1
19.5	95.5 ± 1.5	95.0 ± 1.3	83.7 ± 0.8	96.6 ± 1.3	94.6 ± 1.1	81.1 ± 0.8	93.4 ± 3.9	89.9 ± 2.5	54.6 ± 0.9
20.0	95.5 ± 1.5	94.4 ± 1.2	68.9 ± 0.8	96.0 ± 1.2	93.7 ± 1.1	69.4 ± 0.7	93.2 ± 3.5	88.4 ± 2.1	35.0 ± 0.6
20.5	95.5 ± 1.4	92.4 ± 1.2	28.5 ± 0.4	94.6 ± 1.2	91.4 ± 1.0	28.0 ± 0.4	92.0 ± 3.0	82.4 ± 1.6	9.7 ± 0.3
21.0	95.1 ± 1.4	88.8 ± 1.1	3.0 ± 0.1	94.7 ± 1.2	83.5 ± 1.0	1.6 ± 0.1	88.6 ± 2.5	77.7 ± 1.3	1.1 ± 0.1
21.5	94.7 ± 1.4	84.0 ± 1.0	0.2 ± 0.0	92.0 ± 1.1	74.7 ± 0.9	0.1 ± 0.0	88.1 ± 2.1	69.4 ± 1.1	0.2 ± 0.0
22.0	92.3 ± 1.3	78.5 ± 0.9	0.0 ± –	88.3 ± 1.1	60.5 ± 0.8	–	81.4 ± 1.7	51.4 ± 0.8	–
22.5	89.8 ± 1.2	64.8 ± 0.8	–	80.5 ± 1.0	25.5 ± 0.4	–	78.0 ± 1.4	21.1 ± 0.5	–
23.0	85.2 ± 1.0	31.2 ± 0.5	–	74.9 ± 1.0	2.6 ± 0.1	–	71.6 ± 1.2	3.1 ± 0.2	–
23.5	81.5 ± 1.0	4.6 ± 0.2	–	64.5 ± 0.9	0.1 ± 0.0	–	58.4 ± 1.0	0.2 ± 0.0	–
24.0	72.5 ± 0.9	0.3 ± –	–	40.7 ± 0.7	–	–	36.2 ± 0.7	–	–
24.5	47.4 ± 0.6	–	–	6.9 ± 0.2	–	–	8.2 ± 0.3	–	–
25.0	8.0 ± 0.2	–	–	0.3 ± 0.0	–	–	0.3 ± 0.1	–	–
25.5	0.3 ± 0.0	–	–	–	–	–	–	–	–

Table 4. Calibration equations obtained for the three observing nights. The quoted zero-points include the zero-point adopted by DAOPHOTII (25 mag).

2011 October 20 # of individual CCD images: 184 in *B*, 188 in *V* and 64 in *I*		
Equation	rms	Stars used for each chip (1–4)
$B - b = 2.696 - 0.111 \times (b - v)$	rms 0.01	148, 124, 64 and 164
$V - v = 2.558 - 0.025 \times (b - v)$	rms 0.01	148, 124, 64 and 164
$V - v = 2.558 - 0.032 \times (v - i)$	rms 0.02	93, 118, 86 and 100
$I - i = 2.317 + 0.016 \times (v - i)$	rms 0.02	93, 118, 86 and 100
2011 October 21 # of individual CCD images: 72 in *B*, 72 in *V* and 40 in *I*		
Equation	rms	Stars used for each chip (1–4)
$B - b = 2.715 - 0.107 \times (b - v)$	rms 0.03	61, 99, 78 and 53
$V - v = 2.614 - 0.045 \times (b - v)$	rms 0.03	61, 99, 78 and 53
$V - v = 2.615 - 0.053 \times (v - i)$	rms 0.03	104, 74, 107 and 70
$I - i = 2.368 - 0.014 \times (v - i)$	rms 0.03	104, 74, 107 and 70
2011 October 24 # of individual CCD images: 59 in *B*, 95 in *V* and 63 in *I*		
Equation	rms	Stars used for each chip (1–4)
$B - b = 2.759 - 0.209 \times (b - v)$	rms 0.02	11, 21, 11 and 9
$V - v = 2.606 - 0.075 \times (b - v)$	rms 0.02	11, 21, 11 and 9
$V - v = 2.576 - 0.039 \times (v - i)$	rms 0.03	29, 24, 14 and 16
$I - i = 2.324 + 0.012 \times (v - i)$	rms 0.03	29, 24, 14 and 16

average coefficients $k_B = -0.22$, $k_V = -0.15$ and $k_I = -0.04$ given by the telescope web page for all the three clusters. The results are summarized in Table 4.

Comparing the calibrated *V* obtained from $(b - v)$ with that obtained with $(v - i)$, we find a small difference of $\leq$0.02 mag, which tends to worsen towards fainter magnitudes (see Fig. 2).

In Figs 3–5 we show the comparisons of our calibration with the literature ones (downloaded through WEBDA[3]) for NGC 1817, NGC 2141 and Be 81. In the case of NGC 1817, we find a small offset: about 0.04 mag in *B* and 0.03 mag in *V*, corresponding to an offset of 0.01 mag in $B - V$. More worrisome are the comparisons obtained for NGC 2141 and Be 81, showing an offset of up to 0.1 mag. The explanation for such differences is not straightforward, since we can only perform relative comparisons, with no absolute reference point. There must be issues related to the adopted calibration equations, but it is not possible to identify in which data set. We have further investigated this problem using photoelectric measurements, when available. This was feasible for NGC 1817 and NGC 2141, thanks to the photoelectric data by Harris & Harris (1977), Purgathofer (1964) and Burkhead et al. (1972), but not for Be 81. The results are shown in Fig. 6. The agreement between our

[3] The WEBDA data base is operated at the Department of Theoretical Physics and Astrophysics of the Masaryk University, see http://webda.physics.muni.cz

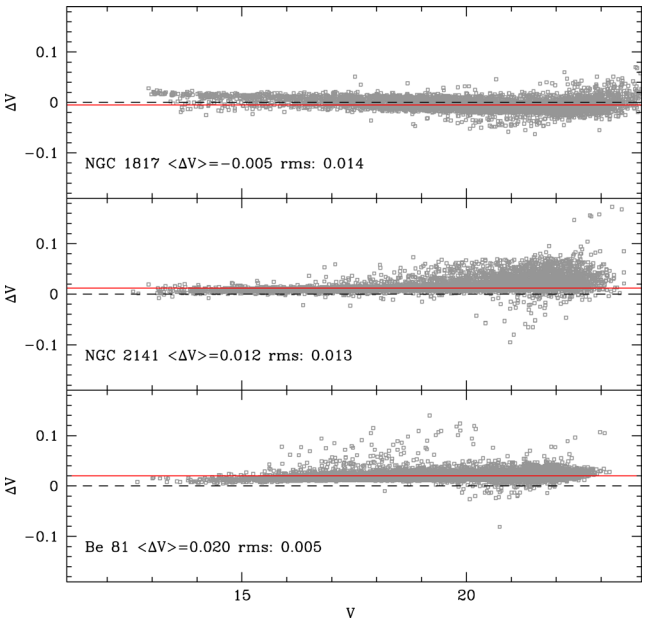

Figure 2. Comparison of the V calibrated from $(b - v)$ and $(v - i)$ colours with respect to the V magnitude for the three clusters (from top to bottom NGC 1817, NGC 2141 and Be 81). The labelled values $\langle \Delta V \rangle$ are the medians of all the stars shown for each plot.

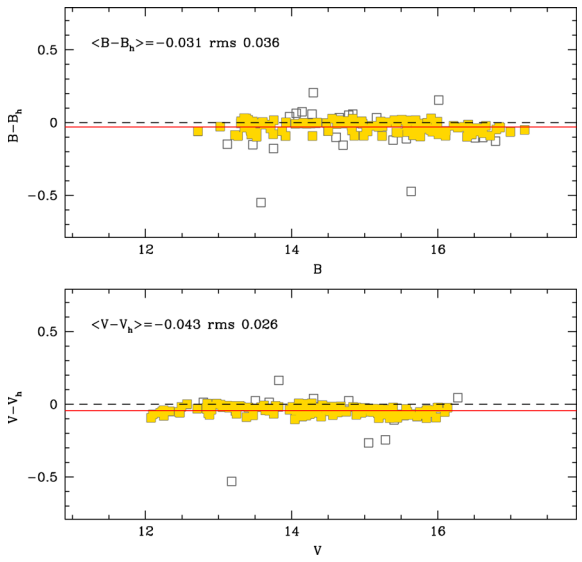

Figure 3. Comparison of our photometry with the one by Harris & Harris (1977) for NGC 1817. The average difference is computed using the golden points, retained after 1σ clipping has been applied.

photometry and photoelectric standards is good for both clusters, showing only a tiny offset, smaller than 0.02 mag in most cases and only slightly worse for the B of NGC 1817.

For NGC 1817 we were also able to compare our photometry with the Sloan Digital Sky Survey (SDSS; see York et al. 2000) using the transformation by Lupton[4] to convert their magnitudes into the Johnson–Cousins system. The results are shown in Fig. 7. The median of the difference in B is about 0.05 mag, and is lower

[4] http://www.sdss.org/dr4/algorithms/sdssUBVRITransform.html#Lupton2005

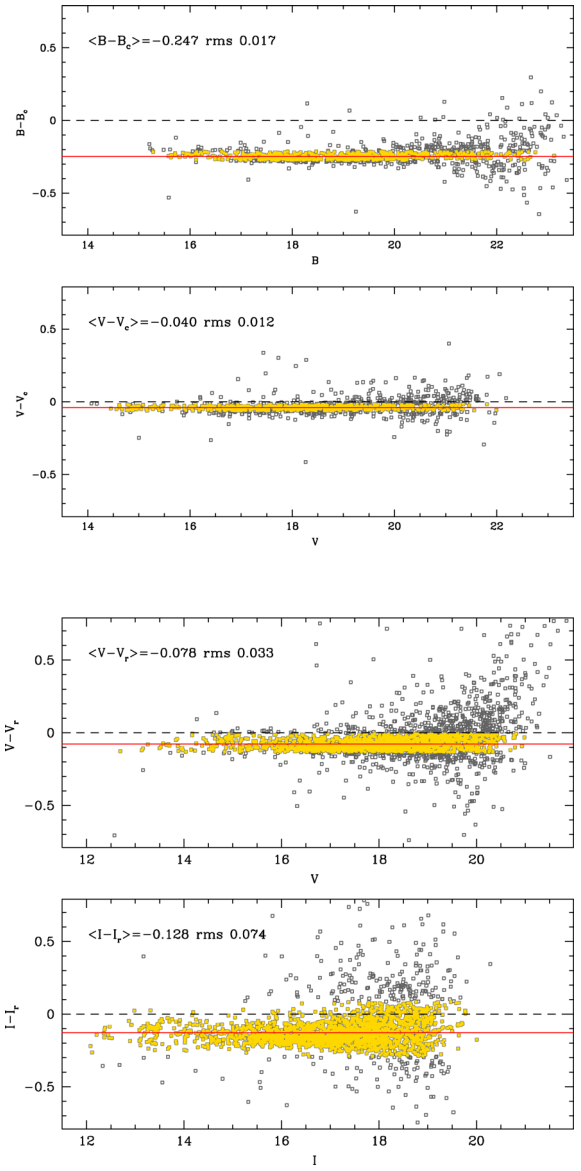

Figure 4. Same as Fig. 3, but for NGC 2141. In the upper panels we compare B and V with the photometry of Carraro et al. (2001), in the bottom panels V and I with Rosvick (1995).

than 0.03 in V and I. This translates in colour differences smaller than 0.03 mag.

In summary, we find that our photometry for NGC 1817 is in good agreement with the literature, and in particular with both photoelectric measurements and SDSS data. For NGC 2141 we find a poor comparison with literature CCD data but a very good agreement with photoelectric measurements, which makes us confident of our results. For Be 81 there were no further checks feasible, but, given the robustness of the calibrations adopted for the other two clusters, we believe the third is correct too.

2.3 The colour–magnitude diagram

The CMDs obtained for the three clusters are shown in Figs 8 and 9, with errors in colour and magnitude indicated. The errors are evaluated using the artificial stars tests. They are random standard errors, with no consideration of possible sources of systematics. In

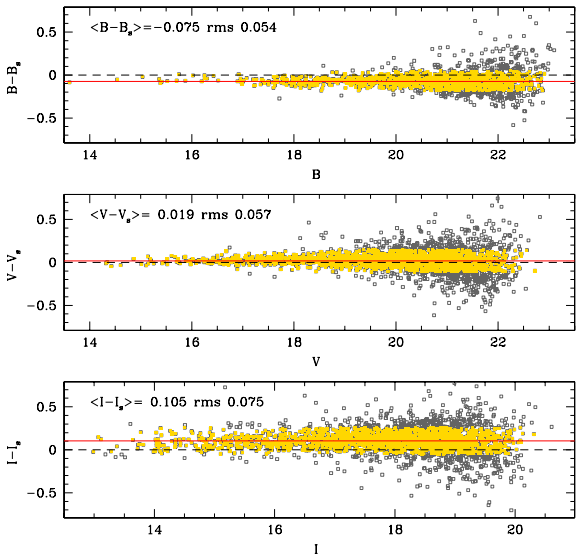

Figure 5. Same as Fig. 3, but for Be81 compared to Sagar & Griffiths (1998).

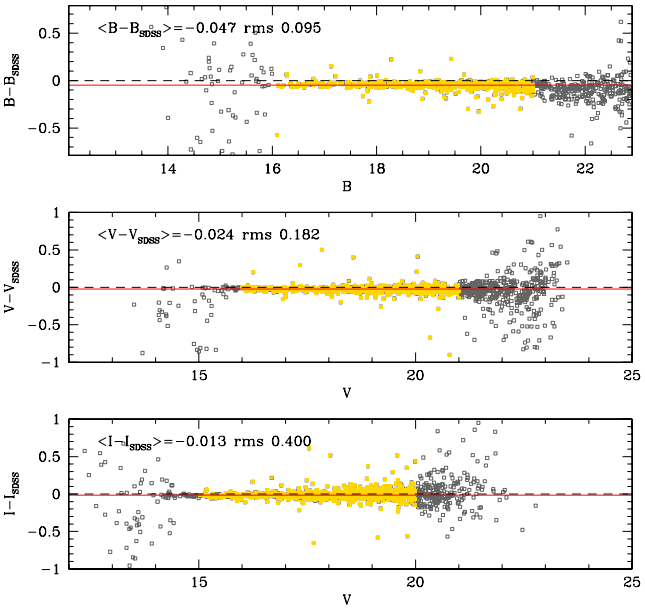

Figure 7. Comparison of the *BVI* with SDSS *ugri* magnitudes calibrated to the Johnson–Cousins system for NGC 1817. The median of the difference (red line) is computed using the golden points: we excluded bright and possibly saturated stars and faint star, we used stars in common only with chip#2 and flagged with *Q* SDSS parameter equal to three.

the upper panels only the more central regions are plotted, while more external regions are used for comparison to estimate the field contamination. For Be 81 the size of the LBC FoV makes this possible, but NGC 2141 is present also in the outer parts of the FoV, and NGC 1817 is so extended that it fills all the four CCDs.

The differences between the CMDs of the three OCs are quite evident.

NGC 1817 is a young and luminous cluster, but not as rich as NGC 2141. Its size is probably larger than the LBT FoV, given the presence of probable cluster RC (at $V \sim 12$ mag) and MS stars in the outer parts of our frames. The brighter MS and RC stars were saturated in I even in short exposures and we miss them in the $V, V - I$ CMD. On the other hand we obtained a very good description of the MS, which extends for about 10 mag in V.

NGC 2141 shows a very rich MS and a populated RC at $V \sim 15$ mag. The red giant branch (RGB) is visible at $B - V \sim 1.6$–2.0 up to $V = 13$ and there are a few probable subgiant branch (SGB) stars at its base. The binary sequence (redder and brighter than the MS) is very clear and neat. The turn-off (TO) is extended in colour, with a 'golf club' shape common to other young OCs (see Section 4). A small clump of stars bluer and brighter than MS stars ($V \sim 15.5$, $B - V \sim 0.3$) is visible, probably blue stragglers.

Be 81 is heavily contaminated by field stars, and is hardly distinguishable, even using the control field for comparison. However, there is a mild excess of stars at $V \sim 16.5$ and $B - V \sim 1.9$, which is not present in the outer field, and can be considered the cluster signature, probably its RC.

The catalogue with the photometry of the three clusters will be made available through the CDS.

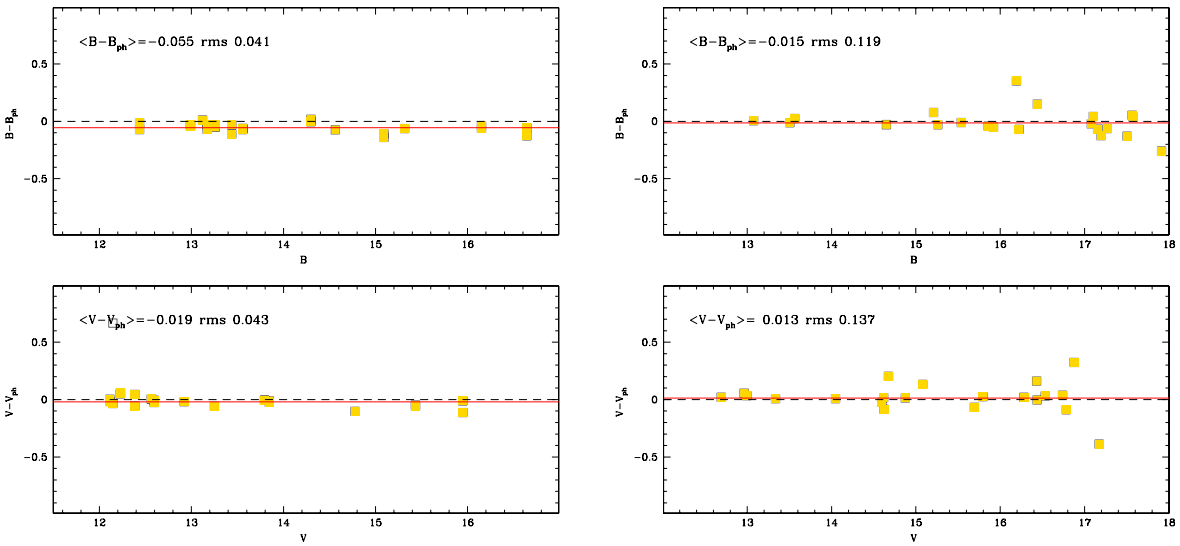

Figure 6. Comparison of the *B* and *V* calibrated photometry with the photoelectric photometry. On the left the results for NGC 1817, on the right the case of NGC 2141.

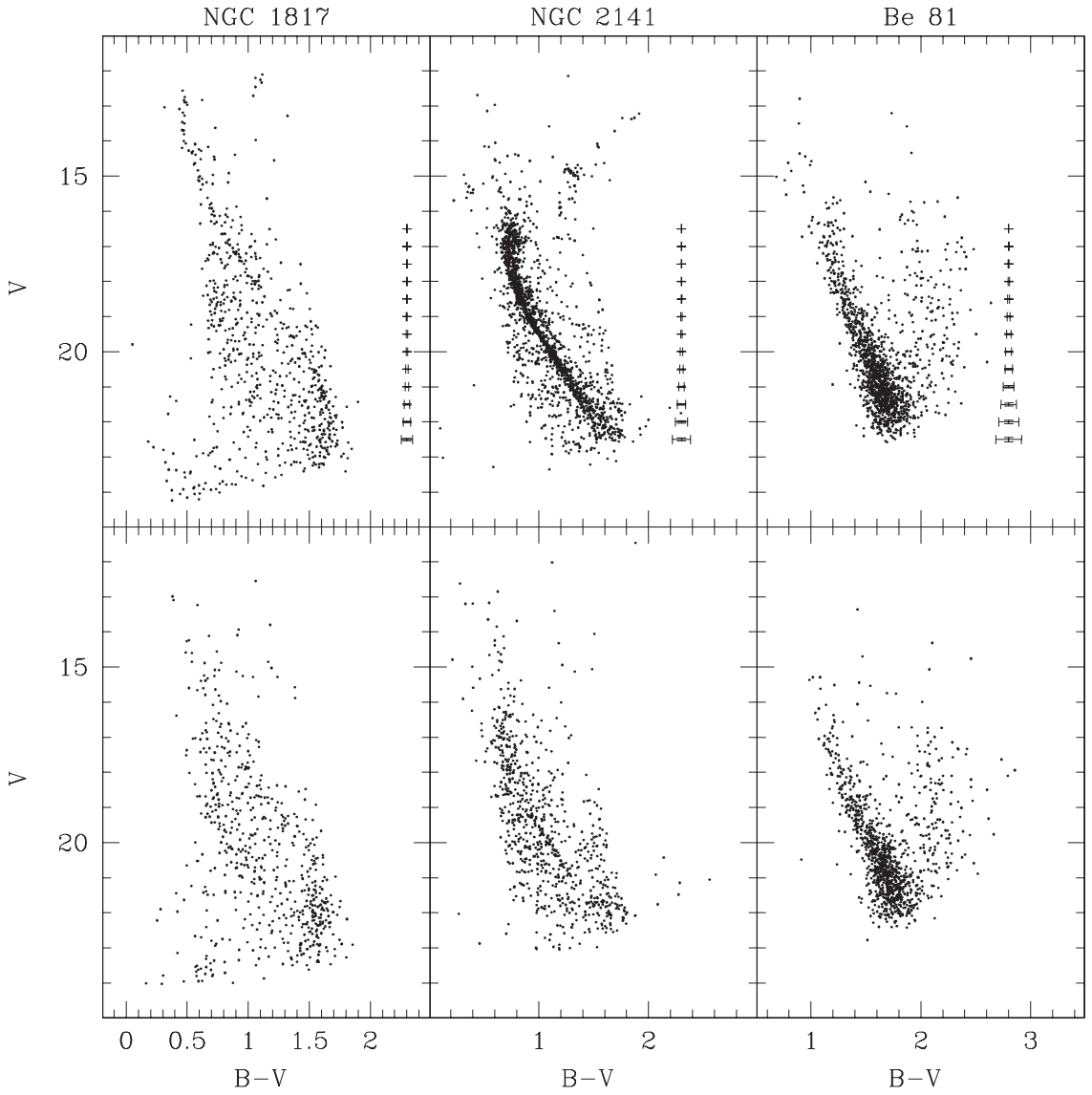

Figure 8. Upper panels: $V, B-V$ CMDs for the inner part of NGC 1817 ($d < 5$ arcmin), NGC 2141 ($d < 3$ arcmin) and Be 81 ($d < 2.5$ arcmin). The errors on colour and magnitudes are indicated by error bars and derived using the artificial stars tests. Lower panels: $V, B-V$ CMDs for an external area with the same dimension.

2.4 Radial velocity

For NGC 1817 and NGC 2141, we have identified the stars in our catalogue with literature RVs from high-resolution spectroscopy. They are all evolved stars, mainly on the RC but also on the bright RGB. They are listed in Table 5, and are displayed with larger symbols in the CMDs of Fig. 10.

For Be 81, Warren & Cole (2009) observed stars in the CaT spectral region, but we opted not to use their data because of the large uncertainty in the membership attribution (see introduction and their section 3.1).

3 CENTRE OF GRAVITY AND DENSITY PROFILE

Exploiting the deep and precise photometry obtained with LBT and its large FoV, we re-determined the centre of each cluster following the approach described in Donati et al. (2012). Briefly, we selected the densest region on the images by looking for the smallest coordinates interval that contains 70 per cent of all the stars. The centre is obtained as the average RA and Dec. when the selection is iterated twice. For a more robust estimate, several magnitude cuts have been considered and the corresponding results averaged. The root mean square (rms) on the centre coordinates is about 5 arcsec.

The most uncertain determination is for NGC 1817. It is a nearby cluster, hence its projected angular dimensions are larger than the LBT's FoV. Moreover, it is not richly populated and it does not seem particularly concentrated, circumstances that both hamper the analysis. We thus applied the same method on the 2MASS catalogue to check the results on a larger FoV (30 arcmin of radius). We find a very similar answer, with a difference of only about half arcminute in both RA and Dec. We therefore adopted the value obtained from our photometry, which is more precise and deeper than 2MASS, and allows us to include stars on the fainter MS. The results are summarized in Table 6.

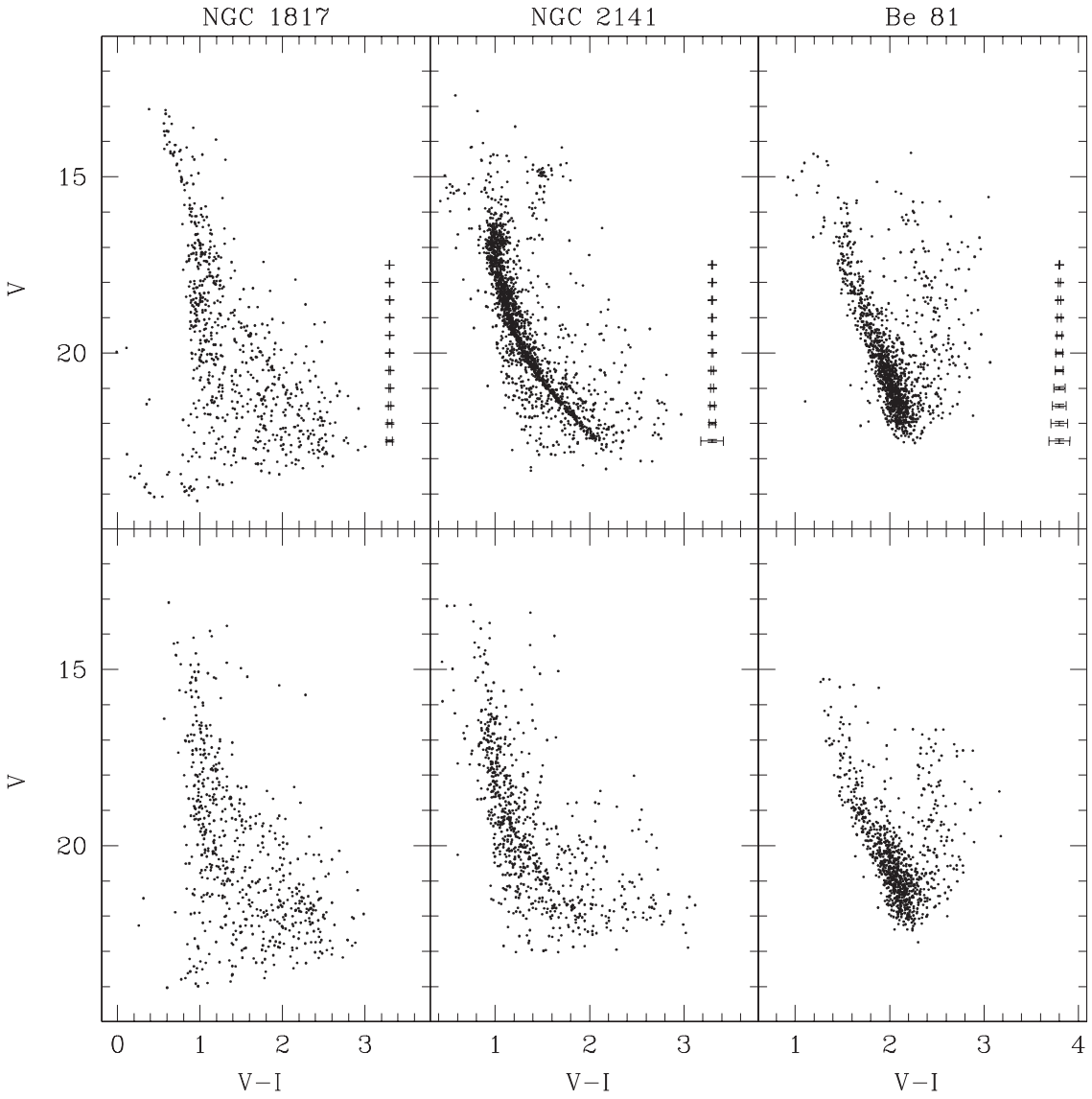

Figure 9. As Fig. 8, but for $V, V-I$.

Following the approach adopted by Cignoni et al. (2011), the projected number density profile is determined by dividing the entire data set in N concentric annuli, each one partitioned in four subsectors (although only two or three subsectors are used, if the available data sample only a portion of the annulus). The number of stars in each subsector is counted and the density is obtained by dividing this value by the sector area. The stellar density in each annulus is then obtained as the average of the subsector densities, and the uncertainty is estimated from the variance among the subsectors. Also in this case, only stars within a limited range of magnitudes are considered in order to avoid spurious effects due to photometric incompleteness.

The observed stellar density profiles are shown in Figs 11 and 12 for the clusters Be 81 and NGC 2141, respectively. For these two OCs the collected data set covers the entire cluster extension, reaching the outermost region where the Galactic field stars represent the dominant contribution with respect to the cluster. This is not the case for NGC 1817, which is not fully covered by the LBT's FoV. As done for the centre determination, we tried to evaluate its density profile on a larger area using 2MASS, SDSS and literature catalogues, but the looseness of the cluster and its proximity to a nearby OC (NGC 1807, even if Balaguer-Núñez et al. 2004b showed that NGC 1807 is not a physical cluster) jeopardize the analysis. Unable to reach a satisfying conclusion, we preferred to limit the analysis to Be 81 and NGC 2141. The results are summarized in Table 6.

In order to reproduce the observed profile, isotropic, single-mass King models (King 1966) have been computed adopting the Sigurdsson & Phinney (1995) code. The best-fitting models are shown as solid curves are shown in Figs 11 and 12 together with the observed density profiles. In each figure we also show the values of concentration ($c = \log_{10}(r_t/r_c)$), core radius (r_c), half-mass radius (r_h) and tidal radius (r_t) as obtained from the best-fitting model. The residual of the fit of the model to each observed point is shown in the lower panel of each density plot.

Clearly, Be 81 is a small, low-mass and very sparse OC. The density profile is hence affected by larger statistical uncertainty. Nevertheless, the residuals of the model fit are quite small, at least in the most central part, where the star counts are dominated by the cluster's members.

Table 5. Stars in common with Jacobson et al. (2009, 2011) and Yong et al. (2005) in NGC 1817 and NGC 2141.

ID	RA	Dec.	V	$B-V$	$V-I$	ID_{webda}	RV	Flag
NGC 1817 – stars in common with Jacobson et al. (2011)								
1429	78.0807757	16.6801860	12.116	1.052	99.999	8	64.8	M
1431	78.0260996	16.6376011	12.232	1.025	99.999	81	65.1	M
1432	78.0190940	16.6740782	12.237	1.227	99.999	90	27.8	NM
1434	78.0271406	16.7457104	12.389	1.048	99.999	177	65.2	M
1435	78.0444686	16.6419862	12.494	1.027	99.999	79	65.8	M
1436	78.0960056	16.5669407	12.480	1.268	99.999	155	14.5	NM
1438	78.0772008	16.6959836	12.597	0.960	99.999	12	62.7	M
1440	78.0941116	16.6357254	12.713	1.034	99.999	40	65.1	M
1448	78.0939209	16.7331841	13.282	1.322	99.999	53	50.4	M?
2922	78.1881838	16.5799475	13.808	0.844	0.976	219	−26.1	NM
3106	78.1092441	16.5988226	12.079	1.039	99.999	72	66.5	M
3108	78.1890040	16.7280692	12.106	1.115	99.999	2049	65.0	M
3109	78.1498523	16.7244935	12.206	1.059	99.999	19	35.2	M?,SB
3110	78.2087521	16.6804613	12.253	1.100	99.999	127	65.1	M
3111	78.1601438	16.7064247	12.336	1.110	99.999	22	63.7	M
3112	78.2283968	16.6160611	12.361	1.126	99.999	2050	65.7	M
3113	78.1356504	16.6660230	12.460	1.059	99.999	30	65.0	M
3116	78.1717679	16.5846748	12.590	1.019	99.999	286	66.9	M
3118	78.2083091	16.7333221	12.710	1.042	99.999	121	64.6	M
3121	78.1291901	16.8236832	12.815	1.055	99.999	185	65.3	M
3124	78.1221863	16.5986027	12.882	1.034	99.999	71	65.9	M
3126	78.1834030	16.6199452	12.931	1.179	99.999	138	8.4	NM
4510	78.3186789	16.6698094	13.663	1.066	1.192	471	48.1	NM
4511	78.2917601	16.7518247	13.468	0.867	0.964	1722	15.1	NM
4513	78.3164620	16.7476535	13.566	0.793	0.929	482	15.6	NM
4518	78.3029299	16.7208041	13.736	0.881	0.955	477	40.3	NM
4670	78.2593664	16.6553140	12.288	1.090	99.999	211	65.1	M
6178	78.0818374	16.9064095	12.235	1.059	99.999	1292	65.5	M
NGC 2141 – [a]Jacobson et al. (2009); [b]Yong et al. (2005)								
6770	90.7115940	10.5078007	13.341	1.761	–	1007[a]	25.5	M
						1007[b]	24.4	M
6590	90.7427760	10.4441398	14.178	1.546	1.715	2066[b]	24.8	M
6604	90.7345371	10.4851441	14.777	1.385	1.606	1286[b]	23.0	M
6644	90.7511372	10.4788874	15.082	1.359	1.572	1333[b]	23.5	M
6771	90.7564588	10.4763049	13.337	1.871	–	1348[b]	24.6	M
6776	90.7500858	10.5398554	14.081	1.500	–	514[b]	23.3	M
6777	90.7814610	10.4469925	14.145	1.537	–	1821[b]	24.8	M

4 DIFFERENTIAL REDDENING

As noted in Section 2.3, NGC 2141 shows a 'golf club' shaped MSTO. We can exclude that this observed feature is due to the photometric error, which is too small to explain the colour extension. Carraro et al. (2001) propose a metallicity spread as best explanation, but this circumstance is very unlikely in OCs. In literature there are other similar examples of Milky Way OCs and Magellanic Clouds clusters showing an extended MSTO (see e.g. Tr 20 in the MW, Platais et al. 2008; and about 10 young globular clusters in the LMC, Milone et al. 2009). Another possible explanation is stellar rotation. For instance, Bastian & de Mink (2009) find that fast rotators at the TO phase have a redder and fainter colour, and can be responsible for the 'golf club' shape. Girardi, Eggenberger & Miglio (2011), instead, exclude that rotation can have such an effect. Also binary systems, which have redder colour and brighter magnitude than single stars, could explain the broadening of the MS, as could an age spread. The latter, however has never been convincingly observed in OCs. A more plausible explanation can be DR. Different absorptions on the cluster field due to different extinction paths along the line of sight results in different shifts in colour and magnitude. This circumstance can also explain the elongated shape of the RC, when RC stars are spread along one single direction.

Most likely, DR is not negligible also over the field of Be 81, that is located very close to the Galactic plane (about 130 pc below the disc, see Section 5) and towards the Galactic Centre. Its high average reddening, $E(B-V) \sim 1.0$ mag, favours the chances for DR. However, Be 81 is severely contaminated by field stars, and this makes it very hard to measure DR. For NGC 1817 there is no direct evidence of DR from the observational CMD (see Fig. 8).

To evaluate the effect of DR for NGC 2141 we adopt the following approach, using a revision of the method described in Milone et al. (2012), adapted to the case of the OCs, which are less populated and more contaminated by field stars than the globular clusters. The main steps of the process are the following.

(i) We draw a fiducial line along the MS, and use it as a reference locus for the DR estimate.

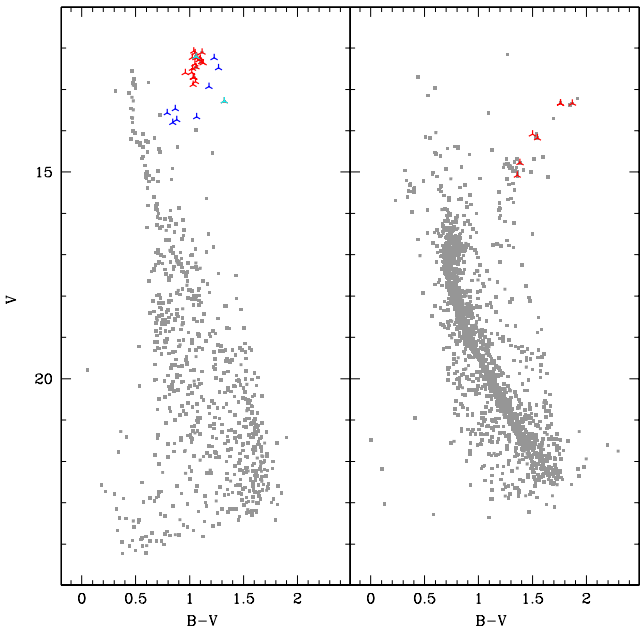

Figure 10. Left-hand panel: CMD of NGC 1817 inside 5 arcmin. Right-hand panel: CMD of NGC 2141 inside 4 arcmin. The shaped points are the targets with RV measurements listed in Table 5. In red the sure members, in blue the non-members and in cyan the stars with uncertain membership.

(ii) We draw a box on the MS: all stars falling in this box are used to estimate the DR. The box is chosen to select stars on the blue side of the MS, and to avoid as many binaries as possible, since they also produce a shift to the red of the sequence. We also keep far from the MSTO and the fainter part of the MS, where errors are larger and field stars confuse the picture.

(iii) For each star in the catalogue we pick the 30 nearest and brightest stars inside the MS box and compute their median distance along the reddening vector direction from the fiducial line in the CMD plane. This distance is used to correct colour and magnitude for DR.

(iv) After the correction for the first DR estimate is applied star-by-star, the algorithm starts a new loop and this procedure is repeated until a convergence is reached. The convergence criterion is a user-defined percentage of stars for which the DR correction is lower than the average rms on these estimates.

(v) Once a final value for the DR is obtained for each star, a binning is performed in the spatial plane. The spatial scale must be compatible with the average distance of the 30 neighbour stars selected and used for the DR estimate. In our case it is less than 1 arcmin^2, as described in the following paragraphs. At this point the outliers are rejected, i.e. stars whose DR estimate is larger than the average error, and stars whose distance to the 30 neighbours is larger than average.

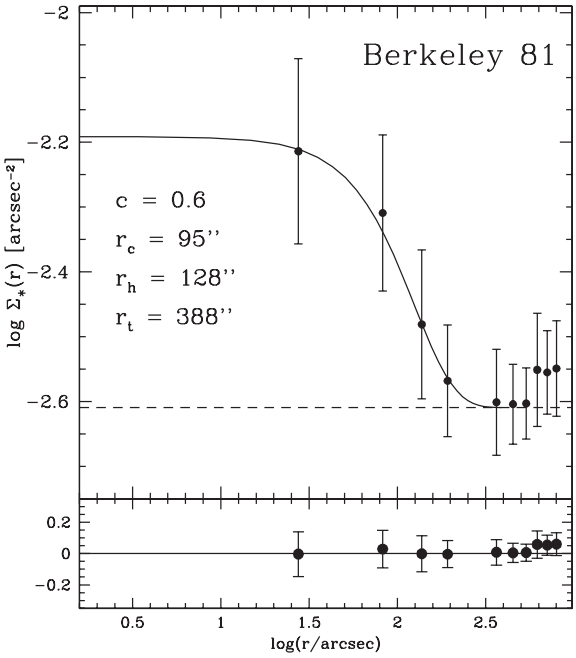

Figure 11. King profile for Be 81.

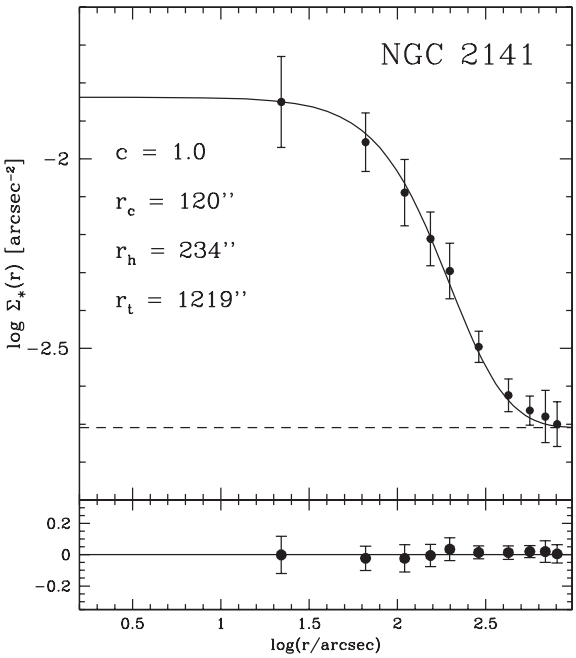

Figure 12. King profile for NGC 2141.

Table 6. Clusters centres and structural parameters. The rms on the centre determination is about 5 arcsec.

Cluster	RA[a] (^{h}:^{m}:^{s})	Dec.[a] ($^{\circ}$:$'$:$''$)	RA (^{h}:^{m}:^{s})	Dec. ($^{\circ}$:$'$:$''$)	c	r_c (arcsec)	r_h (arcsec)	r_t (arcsec)
NGC 1817	05:12:15	16:41:24	05:12:38.33	16:43:48.85	–	–	–	–
NGC 2141	06:02:55	10:26:48	06:02:57.71	10:27:14.43	1.0	120	234	1219
Be 81	19:01:40	−0:27:22	19:01:42.82	−0:27:07.67	0.6	95	128	388

[a]Previous centre estimates from the web update of the Dias et al. (2002) catalogue, see http://www.astro.iag.usp.br/∼wilton/

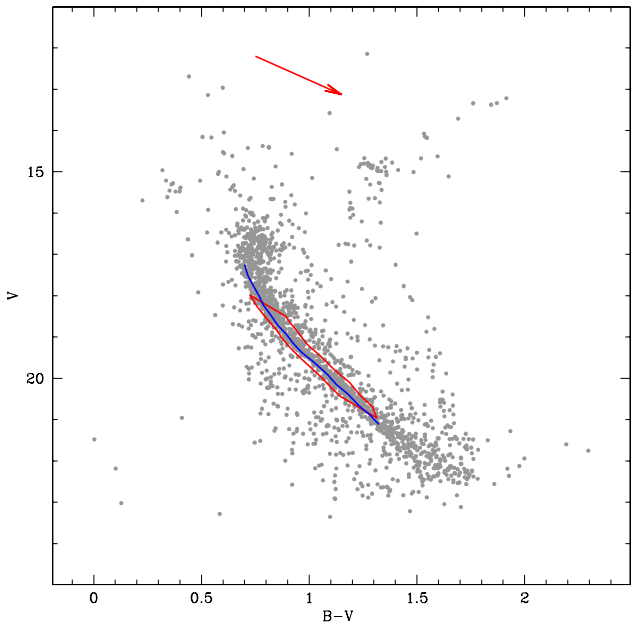

Figure 13. CMD of NGC 2141 inside 4 arcmin. The red box and the blue line indicate the MS box and the fiducial line for the DR estimate. The red arrow indicates the reddening vector.

(vi) A final and robust value for the DR is then computed as the average value of the DR corrections associated with the stars falling in the same bin and the error on this estimate is the associated rms. The values obtained are not absolute values but relative to the fiducial line.

We estimated the DR in the $B - V$ colour. The direction of the reddening vector is derived assuming the standard extinction law [$R_V = 3.1$, $E(V - I) = 1.25\,E(B - V)$] described in Dean, Warren & Cousins (1978). The fiducial line is defined using the CMD of the inner part of the cluster (all the stars inside 4 arcmin) and is chosen as the ridge line along the MS. Several attempts have been made to avoid fiducial lines that, during the estimates of the DR, lead to corrections that artificially and significantly change the magnitude and colour of the age-sensitive indicators (e.g. RC, MSTO). We want in fact to keep RC, MSTO and the blue envelope of the MS as close as possible to the original position in the CMD, to avoid spurious interpretations of the cluster parameters due to DR corrections. When defining the MS box we avoided the broad and bended region of the TO, where the morphology could hamper the correct interpretation, and the fainter part of the MS, where the photometric error is more important. The box and the fiducial line used are highlighted in Fig. 13 with colours.

Taking into account the star counts of the inner and outer parts of the cluster (see Section 3) we decided to limit the DR correction to stars within a 4 arcmin radius (approximately the half-mass radius). For the outer regions the contamination of field stars becomes not negligible (the contrast density counts with respect to the field plateau drops below 50 per cent) and any attempt to estimate the DR is severely affected by field interlopers. The spatial smoothing applied to have a more robust statistic is 0.4×0.4 arcmin^2 in RA and Dec. As final caveat, we stress that photometric errors, undetected binary systems and residual contamination from the field could affect the DR estimation, since they all produce a broadening of the MS. Our results are then an upper limit to the DR.

In Fig. 14 we show the map of the DR obtained in terms of $\Delta E(B - V)$ with respect to the fiducial line. It ranges from ~ -0.04 to $\sim +0.1$. In the same figure we show the corresponding map of the error associated with our estimates. The discrete appearance of these maps is due to two reasons: the poor sampling of a circular area with polygonal bins and the avoidance of interpolation in the corners, where the poor statistics could lead to uncertain estimates.

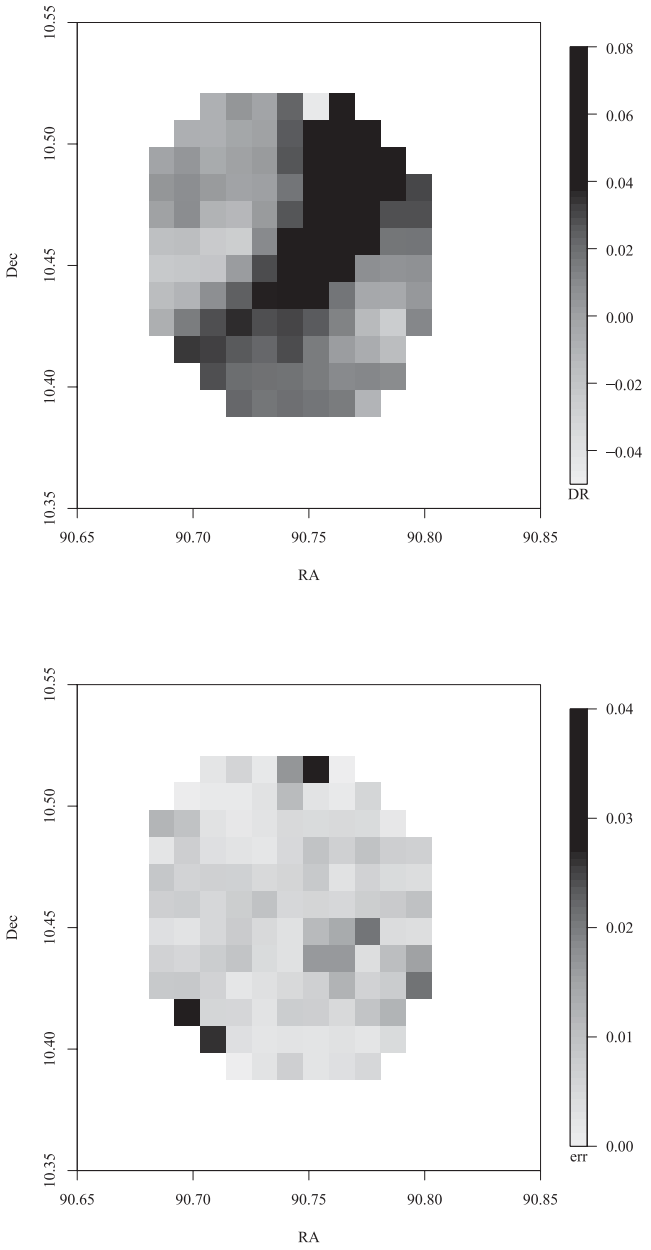

Figure 14. Top panel: colour deviations from the reference line due to the effect of DR, mapped on a 0.4×0.4 arcmin^2 grid for stars inside 4 arcmin from the centre. The correction is expressed in grey-scale colours, see the legend on the right-hand side. Bottom: corresponding error map.

The overall effect of the DR correction on the CMD appearance is shown in Fig. 15. The MS and MSTO region appear tighter, reducing substantially the broadening. In the figure, only the upper MS stars corrected for DR are highlighted in black, but the lower MS benefits from the DR correction too. The RC stars, apparently aligned along the direction of the reddening vector in the original CMD (see the left-hand panel in Fig. 15), appear more clumped after the DR correction, thus supporting the DR hypothesis. Also the RGB looks better defined. Furthermore, our DR estimate does not change the

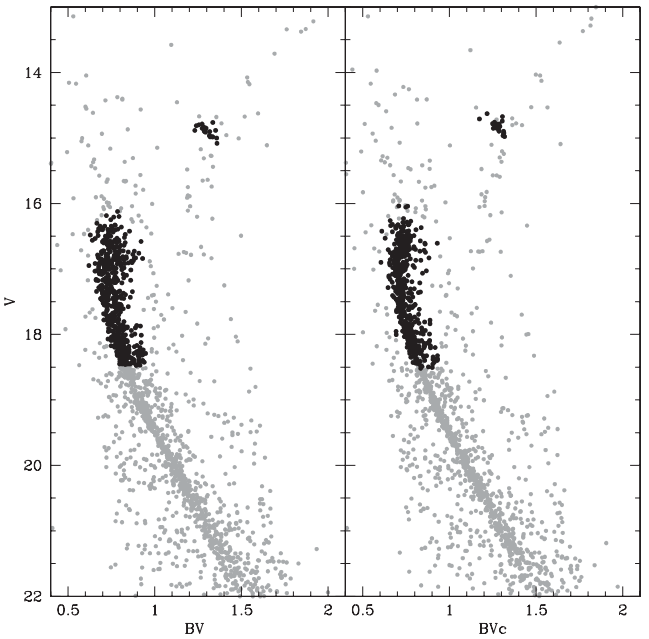

Figure 15. CMDs for NGC 2141 inside 4 arcmin. Left-hand panel: observational CMD. Right-hand panel: CMD after correction for DR. The stars in the upper part of the MS and in the RC phase are highlighted in black to better show the effect of the correction.

luminosity level and colour of age-sensitive indicators such as the MSTO, or the bright edge of the MS, the red-hook phase. We list in our catalogue for NGC 2141 both the original magnitudes and the DR corrected ones.

We cannot apply the same analysis to Be 81 because it is severely contaminated by field interlopers even in the inner regions. For instance, in the central 2 arcmin (approximately the half-mass radius estimated in Section 3), the density contrast is only 25 per cent. Hence, in its case the algorithm would be driven by stars not belonging to the cluster rather than MS stars, seriously weakening the results. We thus prefer to evaluate the effect of DR on Be 81 with the synthetic CMD technique described in the next section.

5 SYNTHETIC CMD

Age, metallicity, distance, mean Galactic reddening and binary fraction have been estimated with the same procedure adopted for other works of this series (see Donati et al. 2012; Ahumada et al. 2013, and references therein). We compare the observational CMDs with a library of synthetic ones, built using synthetic stellar populations (see e.g. Cignoni et al. 2011). Different sets of evolutionary tracks[5] have been used to Monte Carlo generate the synthetic CMDs. The best-fitting solution is chosen as the one that can best reproduce some age-sensitive indicators as the luminosity level of the MS reddest point ('red hook', RH), the RC and the main-sequence termination point (MSTP, evaluated as the maximum luminosity reached after the overall contraction, OvC, and before the runaway to the red), the luminosity at the base of the RGB, the RGB inclination and colour and the RC colour. The most valuable age indicators are the TO point, that is the bluest point after the OvC, and the RC luminosity; however, at least in the case of OCs, these phases may be very poorly populated, and identifying them is not a trivial game, especially if a strong field stars contamination is present (as in the case of Be 81).

The binary fraction is estimated adopting the method described in Cignoni et al. (2011). The DR is taken into account and the synthetic CMD technique applied to the DR corrected photometry. The best fit to all the above indicators provides the best choice for age, reddening and distance modulus. To infer the metallicity it is crucial to analyse together all the *BVI* photometry (see Tosi, Bragaglia & Cignoni 2007): the best metallicity is the one that allows to reproduce at the same time both the observed $B - V$ and $V - I$ CMD. To deal with $(B - V)$ and $(V - I)$ colours we adopted the normal extinction law (Dean et al. 1978).

We estimated the errors on the cluster parameters considering both the instrumental photometric errors and the uncertainties of the fit analysis, as done in Donati et al. (2012). The net effect of the former is an uncertainty on the luminosity level and colour of the adopted indicators. This affects mainly the estimate of the mean Galactic reddening and distance modulus, as they are directly defined by matching the level and colour of the upper MS and the RH and MSTP indicators. We must also consider the dispersion in the results arising from the fit analysis. OCs offer poor statistics, and important indicators, such as the RC locus, are poorly defined. Hence, we cannot find a unique solution, but only a restricted range of viable solutions. In practice, we select the best-fitting synthetic CMD and then take into account the dispersion of the cluster parameters estimates in the error budget. The uncertainties are assumed to be of the form

$$\sigma^2_{E(B-V)} \sim \sigma^2_{(B-V)} + \sigma^2_{\rm fit},$$

$$\sigma^2_{(m-M)_0} \sim \sigma^2_V + R^2_V \sigma^2_{E(B-V)} + \sigma^2_{\rm fit},$$

$$\sigma^2_{\rm age} \sim \sigma^2_{\rm fit}.$$

Typical photometric errors are ∼0.04 on the reddening and ∼0.1 on the distance modulus (assuming negligible the error on R_V). The error resulting from the fit analysis depends mainly on the uncertainty on the RC level and on the coarseness of the isochrone grid. It is of the order of ∼0.02 for the reddening, ranges between 0.01 and 0.05 for the distance modulus and about 0.2–1 Gyr for the age.

5.1 NGC 1817

With the deep LBT photometry we can reach magnitude $V \sim 23$ in the $B - V$ CMD, describing very well the MS. The RC is well visible at $V \simeq 12.3$, as shown in Fig. 16. In the same figure we show the comparison with an external region of the same area. We can see the signature of the cluster (mainly MS stars) also in the outer parts of the image. As explained in Section 3, we could not cover the whole extension of the cluster with the instrument's FoV. There is a clear signature of RC stars, confirmed by the studies on the RV of spectroscopic targets (see Section 2.4 and Fig. 10); the upper part of the MS is poorly populated so it is difficult to reach a statistically firm conclusion on the locus of the RH. We place this phase at magnitude $V \simeq 13$. A well defined binary sequence is visible redward of the MS.

[5] The Padova (Bressan et al. 1993), FRANEC (Dominguez et al. 1999) and FST ones (Ventura et al. 1998) of all available metallicities, as in all the papers of the BOCCE series.

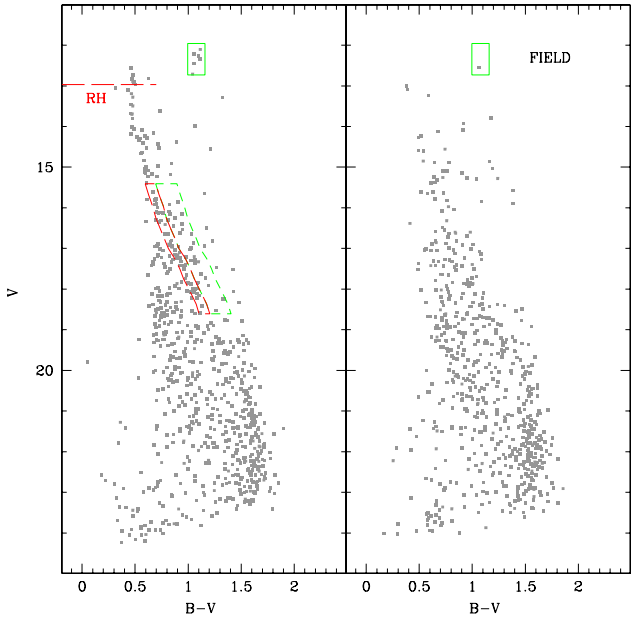

Figure 16. Left-hand panel: $V, B-V$ CMD for the inner part of NGC 1817 (inside 5 arcmin). The age indicators RC (green box) and RH (red line) are shown. The red and green boxes on the MS and redward of it are used to estimate the percentage of binaries. Right-hand panel: CMD of the comparison field of the same area. The same RC box adopted in the left-hand panel is shown here.

To estimate the binary fraction we defined two CMD boxes, one which encloses MS stars and the other redward of the MS in order to cover the binary sequence (see dashed lines in Fig. 16). To remove the field contamination we subtracted the contribution of field stars falling inside the same CMD boxes in a portion of the control field with same area. We performed the same computation on regions smaller and larger than 5 arcmin, finally ending with an estimate between 20 and 30 per cent. The dispersion on the estimate is mostly due to the spatial fluctuations across the control field. For example in the inner area around the cluster centre a higher fraction of binaries is found. Notice that the derived binary fractions may be underestimated, since we possibly miss systems with very low mass secondary, whose luminosity does not alter significantly that of the primary. A mean fraction of 25 per cent has been assumed for all the simulations presented here.

We limit the DR to 0.02 mag because we find no direct evidence of it in this cluster.

After fixing these two parameters we use the synthetic CMD technique to estimate the age, reddening and distance modulus of the cluster. For the simulations we used all the stars inside 5 arcmin from the centre.

Using the Padova models we find that a subsolar metallicity is required to describe with the same model both the $V, B-V$ and $V, V-I$ observational CMDs. In particular the best match is obtained for $Z = 0.008$ ([Fe/H] $\simeq -0.40$), an age of 1.1 Gyr, $E(B-V) = 0.23$ and $(m-M)_0 = 11.1$.

In the case of the FST models we converge to similar results, finding the best solution for a metallicity lower than solar. We chose $Z = 0.01$, an age of 1.05 Gyr, $E(B-V) = 0.21$ and $(m-M)_0 = 10.98$.

For the FRANEC models we find the best fit for $Z = 0.01$, age of 0.8 Gyr, $E(B-V) = 0.34$ and $(m-M)_0 = 10.88$. The age is younger than with the other two models, as expected since these evolution tracks do not include overshooting. We reproduce the magnitude of the age-sensitive indicators (RH and RC), but we do not match the RC colour and the MS shape and colour. In particular, the FRANEC models cannot reproduce the correct inclination of the MS for $V > 16$.

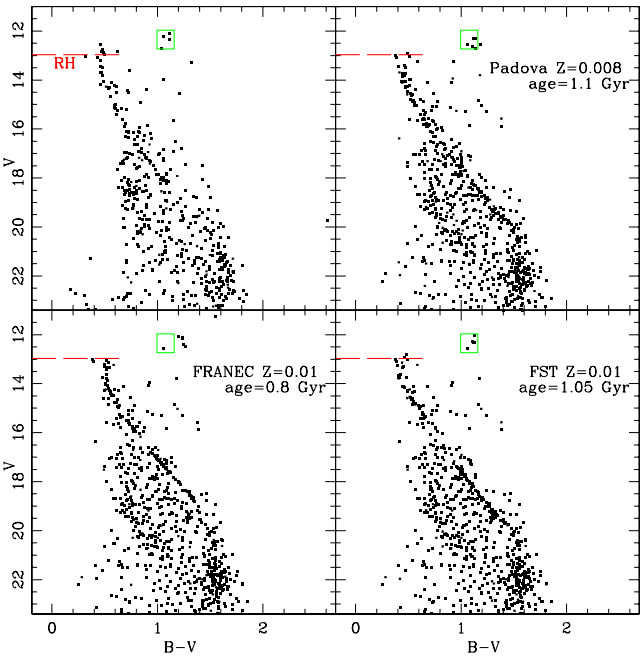

Figure 17. Top left-hand panel: CMD of stars inside 5 arcmin radius area of NGC 1817. Clockwise from the top right-hand panel: the best-fitting synthetic CMD obtained with Padova, FST and FRANEC models.

Fig. 17 shows the comparison between the observational CMD (top left) and the best fits obtained with the three sets of tracks.

The luminosity functions (LFs, see Fig. 18) show a satisfying agreement. There are small departures between the observational

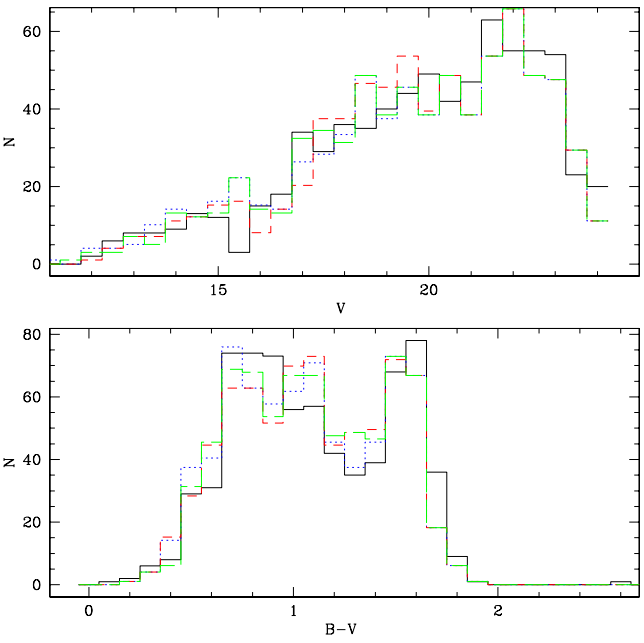

Figure 18. LFs in magnitude V (upper panel) and colour $B-V$ (lower panel). The solid black line is obtained from the observational CMD, the blue dotted line from the Padova synthetic CMD, the red dashed line from the FST synthetic CMD and the green dot–dashed line from the FRANEC synthetic CMD.

Table 7. Cluster parameters derived using different models.

Model	Age (Gyr)	Z	$(m-M)_0$ (mag)	$E(B-V)$ (mag)	$d_\odot$ (kpc)	R^a_{GC} (kpc)	Z (pc)	M_{TO} ($M_\odot$)	M_{tot} ($M_\odot$)
				NGC 1817					
Padova	1.1	0.008	11.10	0.23	1.66	9.61	−373.2	1.8	–
FST	1.05	0.010	10.98	0.21	1.57	9.53	−353.2	1.9	–
FRANEC	0.80	0.010	10.88	0.34	1.50	9.46	−337.3	2.0	–
				NGC 2141					
Padova	1.9	0.008	13.20	0.36	4.37	12.21	−440.9	1.5	5600 ± 300
FST	1.7	0.006	13.06	0.45	4.09	11.95	−413.4	1.6	6160 ± 400
FRANEC	1.25	0.010	13.19	0.45	4.34	12.19	−438.9	1.7	4480 ± 300
				Be 81					
Padova	0.9	0.020	12.40	0.91	3.02	5.74	−131.3	2.1	1540 ± 100
FST	1.0	0.020	12.37	0.90	2.98	5.77	−129.5	2.1	1624 ± 100
FRANEC	0.75	0.020	12.45	0.92	3.09	5.69	−134.4	2.2	1232 ± 100

[a] $R_\odot = 8$ kpc is used to compute R_{GC}.

and synthetic LFs probably due to the poor statistics in star counts. For example the observational CMD (Fig. 16) shows a lack of stars at $V \sim 19$ which is not reproduced in any synthetic CMDs.

From this analysis it turns out that the Padova and FST models provide a better description of the observational CMDs. This restricts the best age to 1.05–1.1 Gyr. Consequently the Galactic reddening is about 0.22,[6] while the distance modulus is between 10.98 and 11.1. The results are summarized in Table 7.

Balaguer-Núñez et al. (2004b) estimate an age of about 1.1 Gyr, a reddening of 0.21 and a distance modulus of 10.9. Our results are in excellent agreement with theirs. The metallicity of the cluster is well defined by several high-resolution spectra analysis, and different works show very similar results of about [Fe/H] $\simeq -0.34$ (see Introduction). Our photometric analysis suggests a metallicity ranging from −0.40 to −0.30 and confirms these findings.

5.2 NGC 2141

NGC 2141 shows clearly all its evolutionary sequences. In Fig. 19 we show the comparison of the inner part of the cluster (inside 4 arcmin, corresponding to the half-mass radius of the cluster) with an external region of the same area. Even in the outer parts of the instrument FoV the cluster is clearly present, with an evident star excess at $V \sim 20$ aligned along the MS direction, and a mild excess at brighter magnitudes. We identify the RH at $V \simeq 16.4$, the MSTP at $V \simeq 16$, the RC at $V \simeq 15$ and $B-V \simeq 1.3$. We find an indication of stars in the SGB phase at the base of the RGB and identify the BRGB at $V \simeq 17$.

We evaluated the fraction of binaries as for NGC 1817, and find an average fraction of 16 per cent. For the simulations we use the photometry corrected for DR (see Section 4), and adopt a DR of 0.02 mag to take into account the intrinsic scatter in the correction.

Keeping fixed these parameters we estimate the cluster age and metallicity comparing the observational CMD for stars inside 4 arcmin from the cluster centre with our synthetic CMDs. We find that only models with metallicity $Z < 0.02$ are in agreement with both $(B-V)$ and $(V-I)$, therefore, we discard models with solar metallicity.

[6] The Schlegel, Finkbeiner & Davis (1998) estimate is 0.43 mag, but this is the asymptotic value in that direction, while the cluster is nearby.

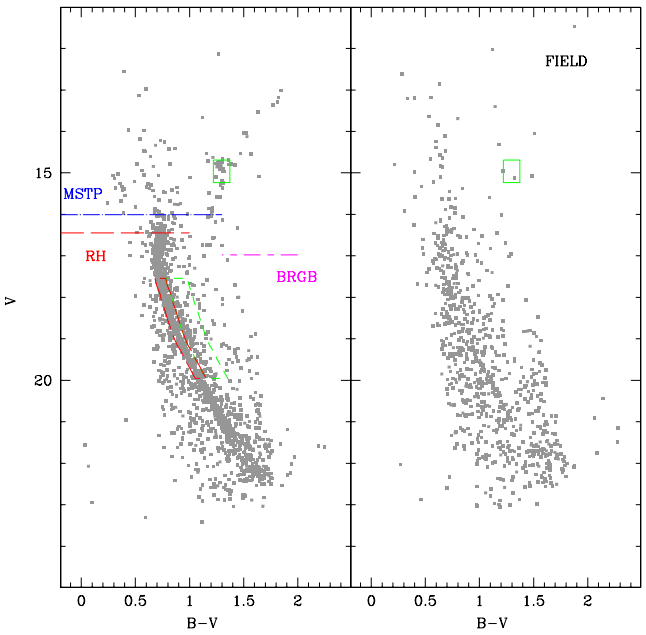

Figure 19. Left-hand panel: $V, B-V$ CMD for the inner part of NGC 2141 (inside 4 arcmin) corrected for DR. The age indicators RC (green box), RH (red line), MSTP (blue line) and BRGB (magenta line) are shown. The red and green boxes on the MS and redward the MS are used to estimate the percentage of binaries. Right-hand panel: CMD of the comparison field of the same area. The cluster is still visible, even if as a minor component.

For the Padova models we obtain the best match using the metallicity $Z = 0.008$ ([Fe/H]∼−0.4). Our synthetic CMD reproduces the magnitude and colour of all the age indicators, reproducing very well the MS, the binary sequence and the RGB. The corresponding cluster parameters are age 1.9 Gyr, $E(B-V) = 0.36$ and $(m-M)_0 = 13.2$.

With the FST models we find a good match for $Z = 0.006$, age 1.7 Gyr, $E(B-V) = 0.45$ and $(m-M)_0 = 13.06$. Also in this case the synthetic CMDs can reproduce well the MS, the binary sequence and the RGB even if the RC colour is slightly redder than observed.

In the case of the FRANEC models, the best fit is obtained for $Z = 0.01$, age of 1.25 Gyr, $E(B-V) = 0.45$ and $(m-M)_0 = 13.19$.

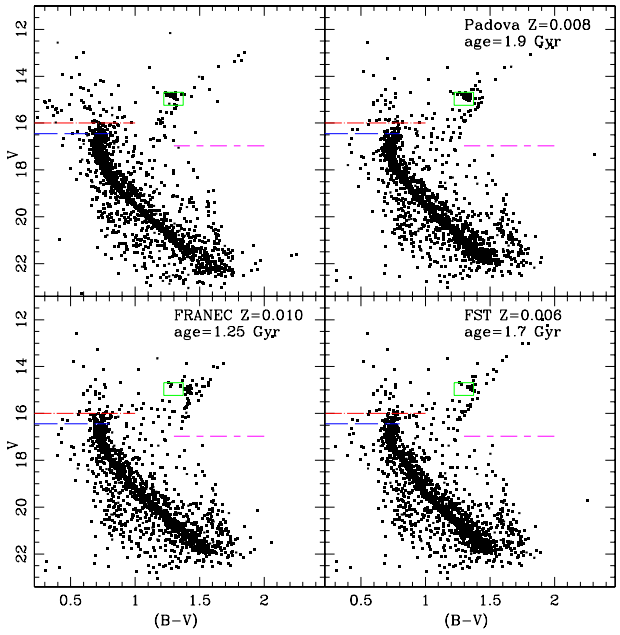

Figure 20. Same as Fig. 17 but for NGC 2141. The observational CMD in the top left-hand panel is for stars inside a 4 arcmin radius area.

Despite being able of matching the luminosity of the age-sensitive indicators, the colour of one of them, the RC, is much redder than observed. Moreover, the MS shape is poorly reproduced for faint magnitudes ($V > 19$).

Fig. 20 shows the comparison between the observed CMD (top left) and the best fits obtained with the three sets of tracks. From this analysis the Padova models provide a better match of the MS shape and of the colour and magnitude of the age indicators. The results are summarized in Table 7.

Looking at the LFs of the observational and synthetic CMDs (see Fig. 21) we clearly see that the peak of the synthetic distribution is fainter than the observational one. In the comparison field (shown in Fig. 19) there are clearly MS stars around $V \sim 20$. This may be due to evaporation, i.e. the typical tendency of low-mass stars of moving out of the cluster. Another possible explanation is related to the initial mass function (IMF). The best model predicts a mass of about 0.8 $M_{\odot}$ at $V \sim 20$, in the mass range where Salpeter's IMF (Salpeter 1955) overestimates the mass fraction. Since the synthetic CMDs are generated assuming Salpeter's IMF, they are likely to overpredict low-mass stars.

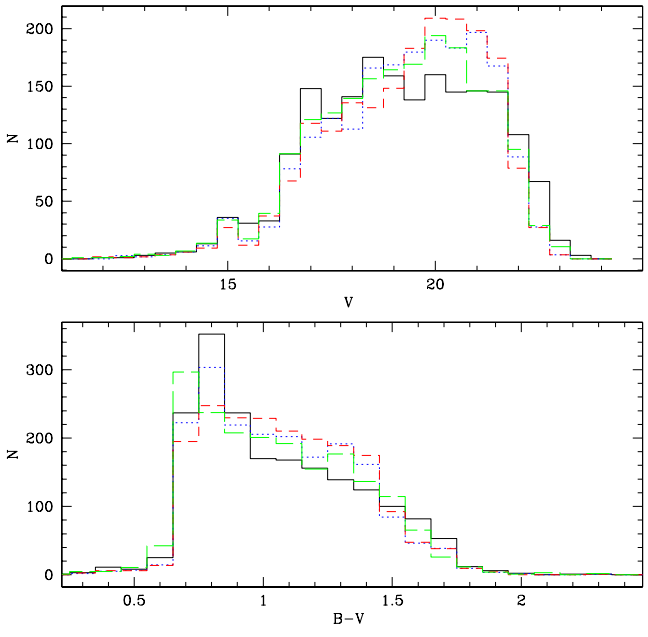

Figure 21. Same as Fig. 17 but for NGC 2141.

Comparing with literature results we find a lower age with respect to both Rosvick (1995) and Carraro et al. (2001). In both cases the authors chose a TO fainter than ours by about 0.5 mag (at about the same level of our RH), and a RC slightly brighter than ours (see fig. 5 in Rosvick 1995). Since the age is primarily constrained by the magnitude difference between the RC and the MSTO, the large difference in age is explained by the choice of these two age indicators. We confirm a subsolar metallicity as suggested by the two papers.

5.3 Be 81

Be 81 is highly contaminated by field interlopers, condition that makes the interpretation of the cluster features more difficult. For a more robust analysis we studied the inner part of the cluster, where the contrast density with respect to the background density (see Section 3) is higher and the cluster members should be more evident. From Fig. 22 an excess at the brighter MS end ($V \simeq 15.6$) and on the probable RC locus ($V \simeq 16.3, B - V \simeq 1.8$) is visible for the central part with respect to an external control region. These features have been evaluated for different inner regions and for different choices of comparison field of the same area. We are confident in adopting these features as age-sensitive indicators.

The binary sequence for this cluster is not evident at all from the CMDs because of the high contamination and possibly DR, and for the simulations we adopted a conservative value of 25 per cent as found on average in many OCs.

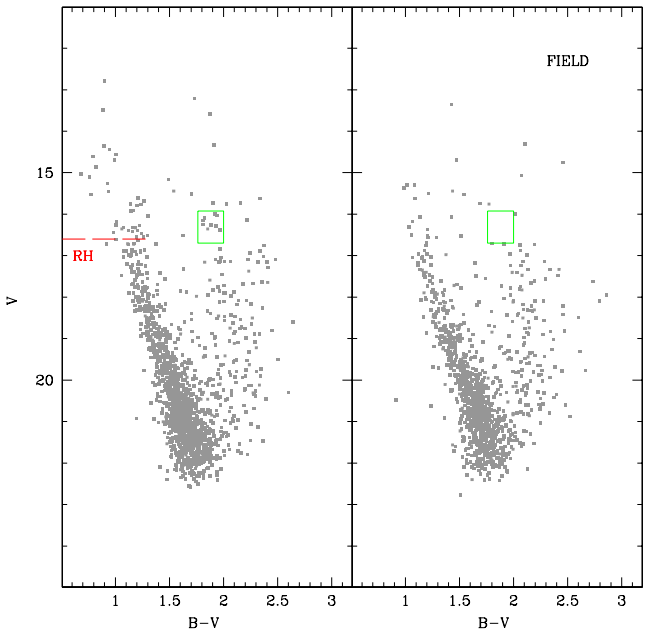

Figure 22. Left-hand panel: $V, B - V$ CMD for the inner part of Be 81 (inside 2 arcmin). The age indicators RC (green box) and RH (red line) are shown. Right-hand panel: CMD of the comparison field of the same area. No RC stars appear in the external part of the field.

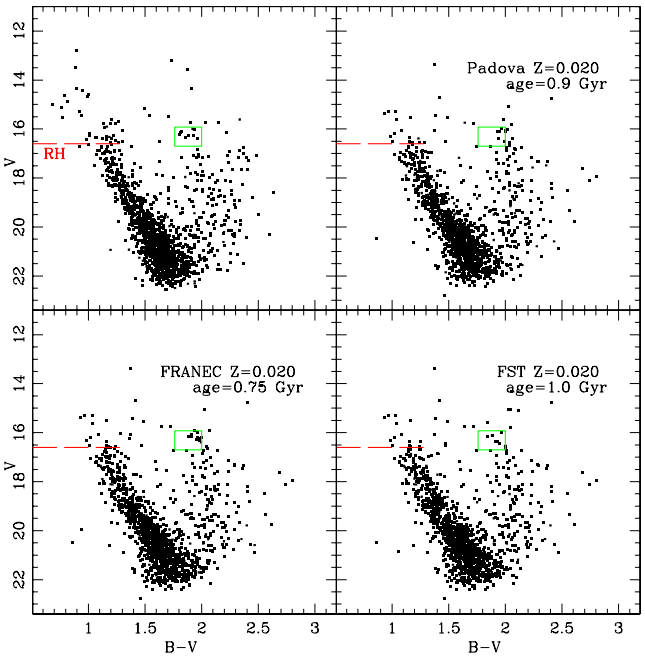

Figure 23. Same as Fig. 17 but for Be 81. The observations CMD in the top left-hand panel is of stars inside a 2 arcmin radius area, corresponding to the half-mass radius of the cluster.

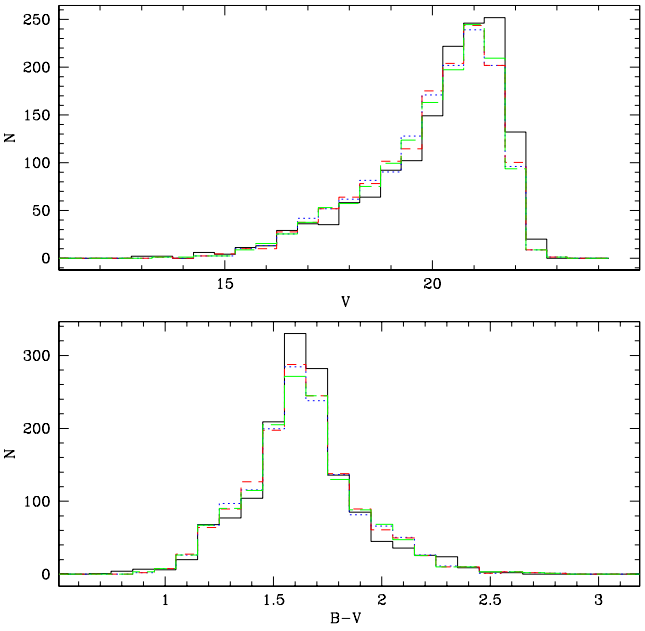

Figure 24. Same as Fig. 17 but for Be 81.

We expect a not negligible DR. The MS appears more extended in colour than expected from the photometric error and the probable RC stars have scattered colour and magnitude. After several tests, we decided to adopt a DR of 0.15 for the simulations, with a sensitivity of 0.03. Lower or higher values imply a too tight or too extended MS in the synthetic CMDs.

We find that the cluster footprints (MS and RC) can be reproduced by a solar metallicity, for which we obtain a good match in both $V, B-V$ and $V, V-I$ CMDs. With all the models we can reproduce the magnitude of the age-sensitive indicators (RH and RC) and the overall shape of the observational CMD (see Fig. 23). The colour of the RC is well recovered by FST and FRANEC models. Because of the high contamination from field stars and the effect of severe DR we cannot detail our analysis further.

With the Padova models we find an age of 0.9 Gyr, an average reddening $E(B-V) = 0.91$ and a distance modulus $(m-M)_0 = 12.4$. In the case of FST models the best match is for an age of 1.0 Gyr, $E(B-V) = 0.90$ and $(m-M)_0 = 12.37$. With FRANEC we estimate an age of 0.75 Gyr, $E(B-V) = 0.92$ and $(m-M)_0 = 12.45$.

The comparison of the observational and synthetic LFs is very good both in magnitude and in colour, as shown in Fig. 24.

We find a good agreement with the results presented by Sagar & Griffiths (1998). We estimate a lower average DR (about 0.1 mag lower) but this can be explained by the differences in our photometries (see Section 2.2). On the other hand they exclude that DR be the explanation of the observed broad MS, pointing out that the severe contamination of field stars pollutes the cluster sequences and drives the CMD appearance. We investigated further this hypothesis using the synthetic CMD technique and choosing different external areas inside our FoV. We find that the lower MS ($V > 19$) is always dominated by field contamination and the signature of the cluster is not evident. Hence we evaluated the DR effect from the brighter part of the MS. It is true that there are many field interlopers even for $V < 19$, but low DRs always imply a too tight synthetic MS and RC with respect to the observations. Hence we suggest that DR is not negligible across the FoV of Be 81. Firmer conclusions, especially on the cluster metallicity, will be obtained from the analysis of the GES spectra. Both RV measurements and chemical abundance estimates will be fundamental to distinguish cluster members from field stars, cleaning the cluster sequences by interlopers.

5.4 The cluster masses

The synthetic CMD technique can also be used to evaluate the total mass of the clusters summing the masses of all the synthetically generated stars still alive. In order to do that properly we normalized the synthetic population to the star counts inside one r_h and with magnitude V for which 100 per cent completeness is achieved. The contamination of field stars is taken into account for the normalization. The derived mass inside one r_h is then multiplied by 2 to have an estimate of the total mass. The results quoted in Table 7 are obtained with Monte Carlo experiments. We generated 300 synthetics for each cluster taking into account the uncertainty on the normalization star counts and the error on the distance modulus and DR parameters. The first one is considered as a Poissonian error on the counts, hence it affects the number of stars extracted to populate the synthetic. The errors on the distance modulus and reddening (quoted in Section 5) affect the mass limit at which the synthetic population is normalized. We use the median of the distribution obtained and its rms as the reference estimate for the total mass of the cluster.

We can perform this evaluation only for NGC 2141 and Be 81, the two clusters for which we could estimate the King profile (see Section 3). For NGC 2141 we adopted $V < 16.75$ as magnitude limit to normalize the synthetic population. This limit corresponds to the faintest magnitude at which completeness is still 100 per cent (see Table 3). For Be 81 we adopted $V < 17.25$ as magnitude limit. Using brighter magnitude limits comparable mass estimates are found within the errors.

These computations provide about $1000\,M_\odot$ for Be 81 and $\sim 4000\,M_\odot$ for NGC 2141. These mass estimates are a lower limit to the total cluster mass. In fact the stellar models we are using to make synthetic populations have a lower mass limit of $0.6\,M_\odot$,

hence all the stars with lower mass are not taken into account. To get the actual cluster mass we then need to extrapolate along the IMF down to 0.1 $M_\odot$. This implies multiplying by a factor of 2 the mass if we adopt Salpeter's IMF (Salpeter 1955) and by a factor of 1.4 if we adopt Kroupa's (2002). Since the latter is supposed to best describe the real IMF, we conclude that Be 81 has a mass of 1400 $M_\odot$ and NGC 2141 of 5600 $M_\odot$. These are the values listed in Table 7.

6 SUMMARY AND CONCLUSIONS

Set in the framework of the BOCCE project (see Bragaglia & Tosi 2006), this paper adds three old OCs to the BOCCE data base. One, Be 81, is located towards the Galactic Centre, while the other two, NGC 1817 and NGC 2141, are in the anticentre direction. They were observed with LBC at LBT using the *BVI* filters. We obtained CMDs 2/3 mag deeper than the ones found in literature; hence we could obtain more precise data for the lower MS. The large instrument FoV allowed us to estimate the structure parameters of the clusters NGC 2141 and Be 81 by fitting a King model to their density profile. The analysis of the cluster parameters was carried out using the synthetic CMDs technique that allowed us to infer a confidence interval for age, metallicity, binary fraction, reddening and distance for each clusters. We used three different sets of stellar tracks (Padova, FST and FRANEC) to describe the evolutionary status of the clusters in order to minimize the model dependence of our analysis. For NGC 2141 a dedicated analysis of the DR is described, using a different technique with respect to the synthetic one and a map of the DR across the cluster is provided. By using the best synthetic CMD and the King profile we evaluated the total cluster mass for NGC 2141 and Be 81. We found the following.

(i) NGC 1817 is located at about 1.6 kpc from the Sun. Its position in the Galactic disc is at $R_{GC} \sim 9.6$ kpc and 360 pc below the plane (assuming $R_\odot = 8$ kpc as in our previous works). The resulting age is between 0.8 and 1.1 Gyr, depending on the adopted stellar model, with better fits for ages between 1.05 and 1.1 Gyr. A metallicity lower than solar seems preferable, in the range $0.006 < Z < 0.010$. The mean Galactic reddening $E(B-V)$ is between 0.21 and 0.34 and we estimate a fraction of binaries of at least 25 per cent.

(ii) NGC 2141 is at ∼4.2 kpc from the Sun, about 12 kpc from the Galactic Centre and ∼430 pc below the Galactic plane. The age is between 1.25 and 1.9 Gyr, with better fits in the age range 1.7–1.9 Gyr. The metallicity for this cluster is lower than solar but higher than $Z = 0.004$; the mean Galactic reddening $E(B-V)$ is about 0.40. The estimated binary fraction for this cluster is ∼16 per cent. For this cluster we evaluated the effect of the DR: its evident structured MSTO phase, resembling a 'golf club' shape common to other MW OCs, and its elongated RC can be explained by the presence of not negligible DR across the cluster. The total mass for NGC 2141 is about 5900 ± 300 $M_\odot$.

(iii) Be 81 is located towards the Galactic Centre at ∼3 kpc from the Sun, and at about 130 pc below the plane. Its Galactocentric distance R_{GC} is 5.7 kpc. This cluster shows a strong contamination by field stars and an extended MS and RC likely due to DR (up to 0.15), adding uncertainty to the interpretation of the cluster parameters. The best-fitting age is between 0.75 and 1.0 Gyr with a preference for models with a solar metallicity. The reddening estimate is $E(B-V) \sim 0.9$. The total mass of this cluster is $\sim 1500 \pm 100$ $M_\odot$.

A robust determination of the three clusters parameters would require additional information on cluster membership for evolved and MSTO stars. This is obtainable in the immediate future measuring RVs of at least many tens of stars, as in the case of Be 81 within the GES, or we can wait for the results of the *Gaia* astrometric satellite, with precise individual distances and proper motions. The estimated metallicity is in concordance with their position on the Galactic disc (lower than solar for the outer disc, and solar for the inner part) but only high-resolution spectroscopy will be able to definitely determine the metallicity value.

Our future plan is to update the study described in Bragaglia & Tosi (2006), adding all new BOCCE clusters (we count now 34 OCs), taking into account the information from our studies, the literature and the on-going surveys, e.g., on metallicity. We will discuss our findings also in the light of improved models of chemical evolution of the disc and taking into account the latest results on stars and clusters migration in the disc.

ACKNOWLEDGEMENTS

We thank Paolo Montegriffo, whose software for catalogue matching we consistently use for our work. This research has made use of the VizieR catalogue access tool, CDS, Strasbourg, France, the WEBDA database, operated at the Department of Theoretical Physics and Astrophysics of the Masaryk University and of Nasa's Astrophysics Data System. We are grateful to the LBC team for the pre-reduction procedures. PD thanks the hospitality of the European Southern Observatory where part of this work was done and the Marco Polo funds of the Università di Bologna.

REFERENCES

Ahumada A. V., Cignoni M., Bragaglia A., Donati P., Tosi M., Marconi G., 2013, MNRAS, 430, 221
Arp H., Cuffey J., 1962, ApJ, 136, 51
Balaguer-Núñez L., Tian K. P., Zhao J. L., 1998, A&AS, 133, 387
Balaguer-Núñez L., Jordi C., Galadí-Enríquez D., Zhao J. L., 2004a, A&A, 426, 819
Balaguer-Núñez L., Jordi C., Galadí-Enríquez D., Masana E., 2004b, A&A, 426, 827
Bastian N., de Mink S. E., 2009, MNRAS, 398, L11
Bellazzini M., Fusi Pecci F., Messineo M., Monaco L., Rood R. T., 2002, AJ, 123, 1509
Bertelli G., Bressan A., Chiosi C., Fagotto F., Nasi E., 1994, A&AS, 106, 275
Bragaglia A., Tosi M., 2006, AJ, 131, 1544
Bressan A., Fagotto F., Bertelli G., Chiosi C., 1993, A&AS, 100, 647
Burkhead M. S., Burgess R. D., Haisch B. M., 1972, AJ, 77, 661
Carraro G., Hassan S. M., Ortolani S., Vallenari A., 2001, A&A, 372, 879
Cignoni M., Beccari G., Bragaglia A., Tosi M., 2011, MNRAS, 416, 1077
Dean J. F., Warren P. R., Cousins A. W. J., 1978, MNRAS, 183, 569
Dias W. S., Alessi B. S., Moitinho A., Lépine J. R. D., 2002, A&A, 389, 871
Dominguez I., Chieffi A., Limongi M., Straniero O., 1999, ApJ, 524, 226
Donati P., Bragaglia A., Cignoni M., Cocozza G., Tosi M., 2012, MNRAS, 424, 1132
Friel E. D., 1995, ARA&A, 33, 381
Friel E. D., Janes K. A., 1993, A&A, 267, 75
Giallongo E. et al., 2008, A&A, 482, 349
Gilmore G. et al., 2012, Messenger, 147, 25
Girardi L., Bressan A., Bertelli G., Chiosi C., 2000, A&AS, 141, 371
Girardi L., Eggenberger P., Miglio A., 2011, MNRAS, 412, L103
Harris G. L. H., Harris W. E., 1977, AJ, 82, 612
Jacobson H. R., Friel E. D., Pilachowski C. A., 2009, AJ, 137, 4753
Jacobson H. R., Pilachowski C. A., Friel E. D., 2011, AJ, 142, 59
King I. R., 1966, AJ, 71, 64
Kroupa P., 2002, in Grebel E. K., Brandner W., eds, ASP Conf. Ser. Vol. 285, Modes of Star Formation and the Origin of Field Populations. Astron. Soc. Pac., San Francisco, p. 86

Landolt A. U., 1992, AJ, 104, 340
Mermilliod J.-C., Latham D. W., Glushkova E. V., Ibrahimov M. A., Batirshinova V. M., Stefanik R. P., James D. J., 2003, A&A, 399, 105
Mermilliod J.-C., Andersen J., Latham D. W., Mayor M., 2007, A&A, 473, 829
Mermilliod J.-C., Mayor M., Udry S., 2008, A&A, 485, 303
Milone A. P., Bedin L. R., Piotto G., Anderson J., 2009, A&A, 497, 755
Milone A. P. et al., 2012, A&A, 540, A16
Minniti D., 1995, A&AS, 113, 299
Parisi M. C., Clariá J. J., Piatti A. E., Geisler D., 2005, MNRAS, 363, 1247
Platais I., Melo C., Fulbright J. P., Kozhurina-Platais V., Figueira P., Barnes S. A., Méndez R. A., 2008, MNRAS, 391, 1482
Purgathofer A., 1961, Z. Astrophys., 52, 186
Purgathofer A., 1964, Ann. Univ. Sternw. Wien, 26, 37
Reddy A. B. S., Giridhar S., Lambert D. L., 2012, MNRAS, 419, 1350
Rosvick J. M., 1995, MNRAS, 277, 1379
Sagar R., Griffiths W. K., 1998, MNRAS, 299, 1
Salpeter E. E., 1955, ApJ, 121, 161
Schlegel D. J., Finkbeiner D. P., Davis M., 1998, ApJ, 500, 525
Sigurdsson S., Phinney E. S., 1995, ApJS, 99, 609
Skrutskie M. F. et al., 2006, AJ, 131, 1163
Stetson P. B., 1987, PASP, 99, 191
Stetson P. B., 1994, PASP, 106, 250
Tosi M., Bragaglia A., Cignoni M., 2007, MNRAS, 378, 730
Ventura P., Zeppieri A., Mazzitelli I., D'Antona F., 1998, A&A, 334, 953
Warren S. R., Cole A. A., 2009, MNRAS, 393, 272
Yong D., Carney B. W., Teixera de Almeida M. L., 2005, AJ, 130, 597
York D. G. et al., 2000, AJ, 120, 1579

This paper has been typeset from a TEX/LATEX file prepared by the author.